HEMODYNAMIC VORTEX ANALYSIS AS A MEANS OF INTRACRANIAL

ANEURYSM RUPTURE PREDICTION

By

Kevin William Sunderland

A DISSERTATION

Submitted in partial fulfillment of the requirements for the degree of

DOCTOR OF PHILOSOPHY

In Biomedical Engineering

MICHIGAN TECHNOLOGICAL UNIVERSITY

2019

This dissertation has been approved in partial fulfillment of the requirements for the

Degree of DOCTOR OF PHILOSOPHY in Biomedical Engineering.

Department of Biomedical Engineering

Dissertation Advisor: *Dr. Jingfeng Jiang*

Committee Member: *Dr. Sean Krikpatrick #1*

Committee Member: *Dr. Gowtham #2*

Committee Member: *Dr. Min Wang #3*

Department Chair: *Dr. Sean Kirkpatrick*

Dedication

To my famliy and friends

who

Contents

List of Figures

List of Tables

Preface

Lorem ipsum dolor sit amet, consectetur adipisicing elit, sed do eiusmod tempor incididunt ut labore et dolore magna aliqua. Ut enim ad minim veniam, quis nostrud exercitation ullamco laboris nisi ut aliquip ex ea commodo consequat. Duis aute irure dolor in reprehenderit in voluptate velit esse cillum dolore eu fugiat nulla pariatur. Excepteur sint occaecat cupidatat non proident, sunt in culpa qui officia deserunt mollit anim id est laborum.

Sed ut perspiciatis unde omnis iste natus error sit voluptatem accusantium doloremque laudantium, totam rem aperiam, eaque ipsa quae ab illo inventore veritatis et quasi architecto beatae vitae dicta sunt explicabo. Nemo enim ipsam voluptatem quia voluptas sit aspernatur aut odit aut fugit, sed quia consequuntur magni dolores eos qui ratione voluptatem sequi nesciunt.

Lorem ipsum dolor sit amet, consectetur adipisicing elit, sed do eiusmod tempor incididunt ut labore et dolore magna aliqua. Ut enim ad minim veniam, quis nostrud exercitation ullamco laboris nisi ut aliquip ex ea commodo consequat. Duis aute irure dolor in reprehenderit in voluptate velit esse cillum dolore eu fugiat nulla pariatur. Excepteur sint occaecat cupidatat non proident, sunt in culpa qui officia deserunt mollit anim id est laborum.

Sed ut perspiciatis unde omnis iste natus error sit voluptatem accusantium doloremque laudantium, totam rem aperiam, eaque ipsa quae ab illo inventore veritatis et quasi architecto beatae vitae dicta sunt explicabo. Nemo enim ipsam voluptatem quia voluptas sit aspernatur aut odit aut fugit, sed quia consequuntur magni dolores eos qui ratione voluptatem sequi nesciunt.

Lorem ipsum dolor sit amet, consectetur adipisicing elit, sed do eiusmod tempor incididunt ut labore et dolore magna aliqua. Ut enim ad minim veniam, quis nostrud exercitation ullamco laboris nisi ut aliquip ex ea commodo consequat. Duis aute irure dolor in reprehenderit in voluptate velit esse cillum dolore eu fugiat nulla pariatur. Excepteur sint occaecat cupidatat non proident, sunt in culpa qui officia deserunt mollit anim id est laborum.

Sed ut perspiciatis unde omnis iste natus error sit voluptatem accusantium doloremque laudantium, totam rem aperiam, eaque ipsa quae ab illo inventore veritatis et quasi architecto beatae vitae dicta sunt explicabo. Nemo enim ipsam voluptatem quia voluptas sit aspernatur aut odit aut fugit, sed quia consequuntur magni dolores eos qui ratione voluptatem sequi nesciunt.

Lorem ipsum dolor sit amet, consectetur adipisicing elit, sed do eiusmod tempor incididunt ut labore et dolore magna aliqua. Ut enim ad minim veniam, quis nostrud exercitation ullamco laboris nisi ut aliquip ex ea commodo consequat. Duis aute irure dolor in reprehenderit in voluptate velit esse cillum dolore eu fugiat nulla pariatur.

Excepteur sint occaecat cupidatat non proident, sunt in culpa qui officia deserunt mollit anim id est laborum.

Sed ut perspiciatis unde omnis iste natus error sit voluptatem accusantium doloremque laudantium, totam rem aperiam, eaque ipsa quae ab illo inventore veritatis et quasi architecto beatae vitae dicta sunt explicabo. Nemo enim ipsam voluptatem quia voluptas sit aspernatur aut odit aut fugit, sed quia consequuntur magni dolores eos qui ratione voluptatem sequi nesciunt.

Lorem ipsum dolor sit amet, consectetur adipisicing elit, sed do eiusmod tempor incididunt ut labore et dolore magna aliqua. Ut enim ad minim veniam, quis nostrud exercitation ullamco laboris nisi ut aliquip ex ea commodo consequat. Duis aute irure dolor in reprehenderit in voluptate velit esse cillum dolore eu fugiat nulla pariatur. Excepteur sint occaecat cupidatat non proident, sunt in culpa qui officia deserunt mollit anim id est laborum.

Acknowledgments

I would like to thank all the members of my committee and my advisor Dr. Jingfeng Jiang. Their leadership, support, knowledge and motivation not only helped me throughout my research, but helped drive me to become a better scientist and to never stop learning.

Special thanks are also needed for Dr. Autumn Schumacher, who was willing to take a gamble on a brand new scientist fresh out of their undergraduate education. Her and expertise (and many hours of manuscript editing) were invaluable in getting me to where I am today.

I would also like to thank my friends for their boundless confidence in me which helped push me through my PhD work. Last but not the least, I would of course like to thank my family. All of their love and support helped make this thesis possible.

Definitions

This provides information on how to write your MS thesis or PhD dissertation using the LaTeX document preparation system in compliance with Michigan Technological University Graduate School requirements.

Lorem ipsum dolor sit amet, consectetur adipisicing elit, sed do eiusmod tempor incididunt ut labore et dolore magna aliqua. Ut enim ad minim veniam, quis nostrud exercitation ullamco laboris nisi ut aliquip ex ea commodo consequat. Duis aute irure dolor in reprehenderit in voluptate velit esse cillum dolore eu fugiat nulla pariatur. Excepteur sint occaecat cupidatat non proident, sunt in culpa qui officia deserunt mollit anim id est laborum.

Sed ut perspiciatis unde omnis iste natus error sit voluptatem accusantium doloremque laudantium, totam rem aperiam, eaque ipsa quae ab illo inventore veritatis et quasi architecto beatae vitae dicta sunt explicabo. Nemo enim ipsam voluptatem quia voluptas sit aspernatur aut odit aut fugit, sed quia consequuntur magni dolores eos qui ratione voluptatem sequi nesciunt.

Lorem ipsum dolor sit amet, consectetur adipisicing elit, sed do eiusmod tempor incididunt ut labore et dolore magna aliqua. Ut enim ad minim veniam, quis nostrud exercitation ullamco laboris nisi ut aliquip ex ea commodo consequat. Duis aute irure

dolor in reprehenderit in voluptate velit esse cillum dolore eu fugiat nulla pariatur. Excepteur sint occaecat cupidatat non proident, sunt in culpa qui officia deserunt mollit anim id est laborum.

Sed ut perspiciatis unde omnis iste natus error sit voluptatem accusantium doloremque laudantium, totam rem aperiam, eaque ipsa quae ab illo inventore veritatis et quasi architecto beatae vitae dicta sunt explicabo. Nemo enim ipsam voluptatem quia voluptas sit aspernatur aut odit aut fugit, sed quia consequuntur magni dolores eos qui ratione voluptatem sequi nesciunt.

Lorem ipsum dolor sit amet, consectetur adipisicing elit, sed do eiusmod tempor incididunt ut labore et dolore magna aliqua. Ut enim ad minim veniam, quis nostrud exercitation ullamco laboris nisi ut aliquip ex ea commodo consequat. Duis aute irure dolor in reprehenderit in voluptate velit esse cillum dolore eu fugiat nulla pariatur. Excepteur sint occaecat cupidatat non proident, sunt in culpa qui officia deserunt mollit anim id est laborum.

Sed ut perspiciatis unde omnis iste natus error sit voluptatem accusantium doloremque laudantium, totam rem aperiam, eaque ipsa quae ab illo inventore veritatis et quasi architecto beatae vitae dicta sunt explicabo. Nemo enim ipsam voluptatem quia voluptas sit aspernatur aut odit aut fugit, sed quia consequuntur magni dolores eos qui ratione voluptatem sequi nesciunt.

Lorem ipsum dolor sit amet, consectetur adipisicing elit, sed do eiusmod tempor incididunt ut labore et dolore magna aliqua. Ut enim ad minim veniam, quis nostrud exercitation ullamco laboris nisi ut aliquip ex ea commodo consequat. Duis aute irure dolor in reprehenderit in voluptate velit esse cillum dolore eu fugiat nulla pariatur. Excepteur sint occaecat cupidatat non proident, sunt in culpa qui officia deserunt mollit anim id est laborum.

Sed ut perspiciatis unde omnis iste natus error sit voluptatem accusantium doloremque laudantium, totam rem aperiam, eaque ipsa quae ab illo inventore veritatis et quasi architecto beatae vitae dicta sunt explicabo. Nemo enim ipsam voluptatem quia voluptas sit aspernatur aut odit aut fugit, sed quia consequuntur magni dolores eos qui ratione voluptatem sequi nesciunt.

List of Abbreviations

ACA   Anterior Communicating Artery

AFI   Aneurysm Formation Indicator

CFD   Computational Fluid Dynamics

DICOM   Digital Imaging and Communications in Medicine

DVO   Degree of Volume Overlap

ENR   Elastic Net Regression

IA   Intracranial Aneurysm

ICA   Internal Carotid Artery

MCA   Middle Cerebral Artery

MLR   Multiple Logistic Regression

NSC   Nearest Shrunken Centroid

OSI   Oscillatory Shear Index

PC-MRI   Phase Contrast Magnetic Resonance Imaging

ROC   Receiver Operator Characteristic

STA-WSS   Spatiotemporaly Averaged Wall Shear Stress

TA-WSS   Temporally Averaged Wall Shear Stress

VMTK   Vascular Modeling Toolkit

VTK   Visualization Toolkit

WSS	Wall Shear Stress
WSSG	Wall Shear Stress Gradient
λ_2	Lambda$_2$
ACL	Access Control List
AIB	Add-In Board
ALE	Arbitrary Lagrangian Eulerian
AMANDA	Advanced Maryland Automatic Network Disk Archiver
AMBER	Assisted Model Building with Energy Replacement
AMD	Advanced Micro Devices
AMOLED	Active-Matrix Organic Light Emitting Diode
AMPI	Adaptive Message Passing Interface
ANL	Argonne National Laboratory
API	Application Program Interface
ASCII	American Standard Code for Information Interchange
ATLAS	Automatically Tuned Linear Algebra Software
b_eff	effective bandwidth Benchmark
BIOS	Basic Input/Output Operating System
BLAS	Basic Linear Algebra Subprograms
BOMD	Born-Oppenheimer Molecular Dynamics
BP	Bootstrap Protocol
CCSR	Center for Computer Systems Research

CentOS	Community enterprise Operating System
CFD	Computational Fluid Dynamics
CHARMM	Chemistry at HARvard Macromolecular Mechanics
CHAMBER	CHarmm $\leftrightarrow$ AMBER
CMake	Cross Platform Make
CODINE	Computing in Distributed Networked Environments
CP2K	Car-Parrinello 2000
CPMD	Car-Parrinello Molecular Dynamics
CPU	Central Processing Unit
CSS	Central Security Service
CTM	Chemical Transport Model
CUDA	Compute Unified Device Architecture
CUDPP	CUDA Data-Parallel Primitives Library
DAE	Differential Algebraic Equation
DARPA	Defense Advanced Research Projects Agency
DAE	Delay Differential Equation
DFT	Discrete Fourier Transform
DFT	Density Functional Theory
DGEMM	Double Precision GEneralized Matrix Multiplication
DHCP	Dynamic Host Configuration Protocol
DMCA	Digital Millennial Copyright Act

DOD	Department of Defense
DOE	Department of Energy
DRM	Distributed Resource Manager
DRMAA	Distributed Resource Manager Application API
EFF	Electron Force Field
EVL	Electronic Visualization Laboratory
FCA	Fabric Collectives Accelerator
FEA	Finite Element Analysis
FFT	Fast Fourier Transform
FFTW	Fastest Fourier Transform in the West
FLOPS	Floating Point OPerations per Second
FPU	Floating Point Unit
FSI	Fluid Structure Interaction
FTDT	Finite Difference Time Domain
FTP	File Transfer Protocol

Abstract

This provides information on how to write your MS thesis or PhD dissertation using the LaTeX document preparation system in compliance with Michigan Technological University Graduate School requirements.

Lorem ipsum dolor sit amet, consectetur adipisicing elit, sed do eiusmod tempor incididunt ut labore et dolore magna aliqua. Ut enim ad minim veniam, quis nostrud exercitation ullamco laboris nisi ut aliquip ex ea commodo consequat. Duis aute irure dolor in reprehenderit in voluptate velit esse cillum dolore eu fugiat nulla pariatur. Excepteur sint occaecat cupidatat non proident, sunt in culpa qui officia deserunt mollit anim id est laborum.

Sed ut perspiciatis unde omnis iste natus error sit voluptatem accusantium doloremque laudantium, totam rem aperiam, eaque ipsa quae ab illo inventore veritatis et quasi architecto beatae vitae dicta sunt explicabo. Nemo enim ipsam voluptatem quia voluptas sit aspernatur aut odit aut fugit, sed quia consequuntur magni dolores eos qui ratione voluptatem sequi nesciunt.

Lorem ipsum dolor sit amet, consectetur adipisicing elit, sed do eiusmod tempor incididunt ut labore et dolore magna aliqua. Ut enim ad minim veniam, quis nostrud exercitation ullamco laboris nisi ut aliquip ex ea commodo consequat. Duis aute irure

dolor in reprehenderit in voluptate velit esse cillum dolore eu fugiat nulla pariatur. Excepteur sint occaecat cupidatat non proident, sunt in culpa qui officia deserunt mollit anim id est laborum.

Sed ut perspiciatis unde omnis iste natus error sit voluptatem accusantium doloremque laudantium, totam rem aperiam, eaque ipsa quae ab illo inventore veritatis et quasi architecto beatae vitae dicta sunt explicabo. Nemo enim ipsam voluptatem quia voluptas sit aspernatur aut odit aut fugit, sed quia consequuntur magni dolores eos qui ratione voluptatem sequi nesciunt.

Lorem ipsum dolor sit amet, consectetur adipisicing elit, sed do eiusmod tempor incididunt ut labore et dolore magna aliqua. Ut enim ad minim veniam, quis nostrud exercitation ullamco laboris nisi ut aliquip ex ea commodo consequat. Duis aute irure dolor in reprehenderit in voluptate velit esse cillum dolore eu fugiat nulla pariatur. Excepteur sint occaecat cupidatat non proident, sunt in culpa qui officia deserunt mollit anim id est laborum.

Sed ut perspiciatis unde omnis iste natus error sit voluptatem accusantium doloremque laudantium, totam rem aperiam, eaque ipsa quae ab illo inventore veritatis et quasi architecto beatae vitae dicta sunt explicabo. Nemo enim ipsam voluptatem quia voluptas sit aspernatur aut odit aut fugit, sed quia consequuntur magni dolores eos qui ratione voluptatem sequi nesciunt.

Chapter 1

Introduction

Subarachnoid hemorrhage is a potentially devastating pathologic condition in which bleeding between the brain and the tissues that cover the brain. One of the prevalent pathologic conditions that may result in subarachnoid hemorrhage is the rupture of an intracranial aneurysm (IA)

Research has shown that there may be a wide array of risk factors that impact IA rupture [**?**].

Lorem ipsum dolor sit amet, at qui viderer recusabo aliquando, dignissim evertitur ei his. Ignota iuvaret fabulas ei vim. Ne utinam inciderint quo. Pri ea congue postulant conclusionemque. Ut elitr dicam elaboraret pro, ius altera voluptaria cu. Eam mazim aliquip cu, recusabo pericula accommodare at mea, facer affert nonumes qui ea.

Discere dissentiet vel et, soluta nostrum epicurei ad eam, cu has aperiam vituperata. In prima quaeque diceret pri. Enim labores contentiones eos at, duo altera denique nominavi ea, eos inani nominavi consectetuer at. Ut elitr dicam elaboraret pro, ius altera voluptaria cu. Eam mazim aliquip cu, recusabo pericula accommodare at mea, facer affert nonumes qui ea. [28, 37, 39]

Section 1

At vix indoctum disputando. Eam cu doctus reprimique, quaeque democritum an eos, sit veniam facete dissentias id. Tale volumus eos te, an eum nulla tincidunt. Mea id recteque theophrastus.

Eirmod malorum vis ei. Choro euismod incorrupte in vim, ludus ornatus vis ex. Hinc wisi impedit eum no, vocent definiebas referrentur in quo. Sanctus vulputate repudiandae usu ut.

Objective

Although there exists a number of studies[16, 134, 146] and methodologies[44, 55] that attempt to assess IAs at a high risk of rupture, inconsistencies between study outcomes leave the development of an ideal predictive model out of reach. In addition,

many of these previous studies assess the geometric[1, 78, 134] and/or hemodynamic wall stressors[16, 102, 146] as a means to predict IA rupture, with limited quantitative assessment of the hemodynamic flow conditions within the aneurysm. **The primary objective** of this work is to assess the viability of adapting quantitative analysis of hemodynamic flow patterns, specifically swirling flow pattern(s) (vortex), within IAs to improve the prediction and understanding of IA rupture. In this work, an overview of recent theories concerning
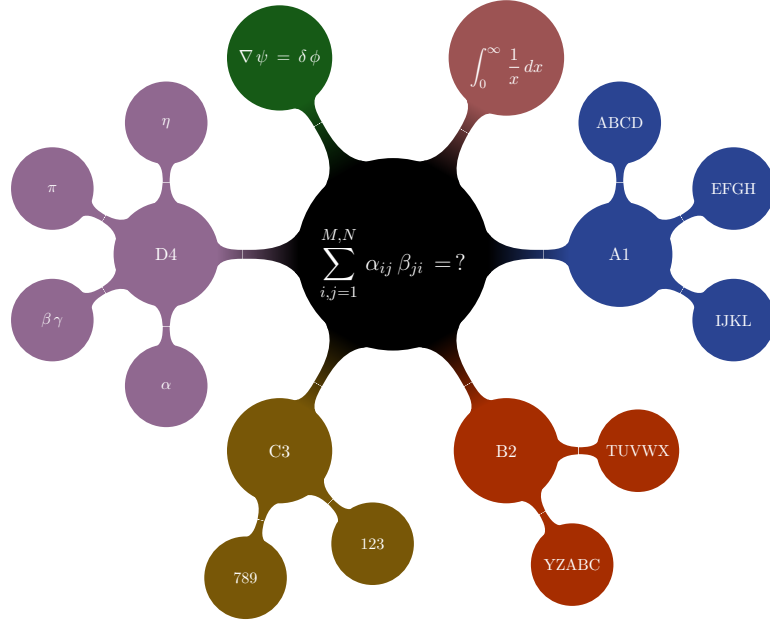
Figure 1.1: Schematic representation of our universe

Methodolgy

For the initial focus of this work, image-based computational fluid dynamics models of patient-specific IA geometry will be constructed from 3D phase contrast magnetic resonance imaging (PC-MRI). Computational fluid dynamic (CFD) simulations will be performed on the computational models to generate realistic 3D hemodyanmic velocity and flow pattern data. From said data,

Figure 1.2: Mathematical functions plotted using TikZ package

Simul noster voluptaria eam ei, sint regione pri ei. Cum no utinam equidem, falli bonorum prodesset an qui. Alterum dissentiet vituperatoribus te eam, eos ea suas oblique. Per ea utinam facilisi. [29, 35, 36] Per iudico probatus complectitur et, cum tollit atomorum rationibus ea.

Aneurysm Geometic Characterisitcs

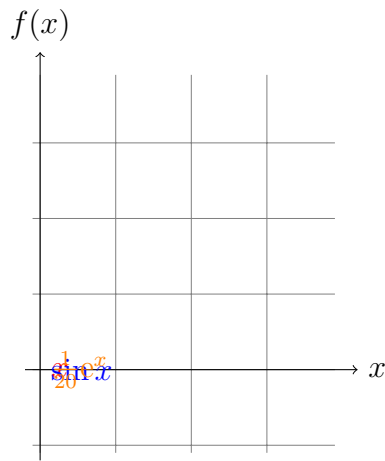All aneurysm geometries were taken from the finalized computational mesh generated for simulations. The aneurysm sac was manually isolated from the parent vessel and the resultant cut plane was capped and identified as the IA ostium using an in-house script written in VMTK. Geometric measurements were either taken directly from the values reported in the Aneurisk dataset, or were calculated using in-house scripts in VMTK.

Aneurysm Surface Area and Volume: Measured directly from the isolated IA geometry before and after (respectively) ostium capping. A number of studies have eluded to an increase in IA size as a risk for both IA growth and rupture. [6, 13, 55, 134]. A meta-analysis performed by Brinjikji et al reported that IA $\leq$ 10 mm in size (diameter) grew at a rate $<$ 2.9% per year, while IAs $>$ 10 mm were associated with growth rates of 9.7% per year. This growth was also reported with an associated IA rupture rate: 3.1% per year compared with 0.1% per year for stable (non-growing) aneurysms (p $\leq$ 01). From a clinical perspective, the overall size of an aneurysm is often a characteristic used to determine course of IA treatment (or lack thereof) [84, 138]. Yet while large IAs are thought to increase the likelihood of rupture, a not-insignificant number of small IAs ($<$5 mm diameter) also have been shown to rupture [74, 78, 85]. This disparity between sizes of ruptured IAs suggest that the

assessment of additional factors in tandem with IA size improve rupture prediction.

Aneurysm Height: The length of the centerline of the IA sac is measured, following the IA shape, as opposed to measuring a straight line from the ostium centroid directly to the highest IA point. The radius of the maximum inscribed sphere at the centerline's furthest point is added to the length measurement to fully measure the IA height. This is a modified version of the typical IA height measurement: a straight line of the maximum stretch from the ostium centroid to the IA dome [41, 96].

Vessel Diameter: The parent artery diameter value is computed at locations close to the aneurysm ostium. For side-wall aneurysms only the location prior to the aneurysm is used. For terminal aneurysms, the vessel diameter along the common branch and both daughter arteries are measured and averaged.

Inlet Cross-sectional Area: The beginning of the inlet vessel was cut square in the 3-matic software package, the resultant cross-sectional area of the inlet vessel was calculated.

Aspect Ratio*: A modified calculation of the commonly defined aspect ratio (aneurysm hight/ostium diameter) was used adapting the sac centerline (SC) length as a measure of aneurysm height [111].

$$AspectRatio* = (SC_{length}/(4*(Ostium_{area}/Ostium_{circumfrence}))) \qquad (1.1)$$

Aneurysm Hemodynamic Characterisitcs

<u>Wall Shear Stress</u>: The calculation of wall shear stress (WSS) is performed by the ANSYS-FLUENT commercial finite-element solver (ANSYS v17.0). The value is defined as the normal velocity gradient against the (vessel) wall:

$$\tau_w = \mu \frac{\partial v}{\partial n} \tag{1.2}$$

with μ as the fluid dynamic viscosity (0.004 kg/m-s).

The spatial-temporally averaged value of the aneurysm's WSS was calculated alongside its temporally-averaged WSS minimum and temporally-averaged WSS maximum.

<u>Kinetic Energy Density</u>:

Docendi eligendi sit et, pri ea dicam eligendi percipitur, has soleat dolores convenire te. Sed altera placerat an, id verterem abhorreant interesset mea. Eum at ceteros efficiantur. Eos id voluptaria efficiendi comprehensam. [37, 38]

In mel modo dicam vocibus, eruditi consectetuer vim no, cu quaestio instructior eum. Justo nostrud fuisset ea mea, eam an libris repudiandae vituperatoribus. Est choro corrumpit definitionem at. Vel sint adhuc vocibus ea, illud epicuri eos no. Sea simul
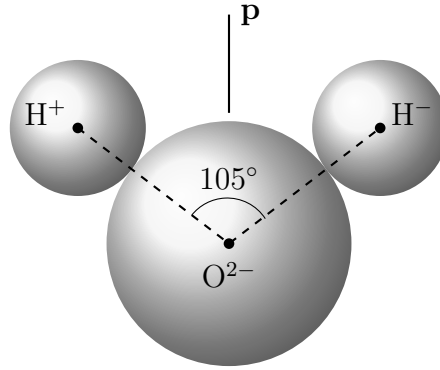
Figure 1.3: Schematic representation of a water molecule

officiis ea, et qui veri invidunt appellantur. Vix et eros ancillae pertinax. [45, 53, 54, 64, 112] Per iudico probatus complectitur et, cum tollit atomorum rationibus ea. Per iudico probatus complectitur et, cum tollit atomorum rationibus ea.

Aliquip lobortis ei est, at error viris graeco sed. Vel te elitr detracto, modo graecis scripserit ex nec. Errem utamur viderer per no, eam ea eripuit referrentur. Pro te dicat disputando. Per iudico probatus complectitur et, cum tollit atomorum rationibus ea. [107, 115, 118, 124]. Per iudico probatus complectitur et, cum tollit atomorum rationibus ea.

Per iudico probatus complectitur et, cum tollit atomorum rationibus ea. Docendi eligendi sit et, pri ea dicam eligendi percipitur, has soleat dolores convenire te. Per iudico probatus complectitur et, cum tollit atomorum rationibus ea.

Chapter 2

Hemodynamic Flow Vortex

Identification

$$\nabla \vec{u} = S + \Omega$$

$$S = \frac{1}{2}\left[(\nabla\vec{u}) + (\nabla\vec{u})^T\right] \qquad (2.1)$$

$$\Omega = \left[\frac{1}{2}(\nabla\vec{u}) - (\nabla\vec{u}^T)\right]$$

Where $\nabla\vec{u}$ is the calculation of the velocity gradient: S as the rate-of-strain tensor and Ω as the vorticity tensor.

Hunt, Wray and Moin [69] defined a vortex as the spatial region of flow where the

Euclidean norm of the vorticity tensor dominates.

$$Q = \frac{1}{2} \left[|\Omega|^2 - |S|^2 \right] > 0 \qquad (2.2)$$

Jeong and Hussain identified the vortices as:

$$\lambda_2 = (S^2 + \Omega^2) < 0 \qquad (2.3)$$

where $\lambda_2 A$ identifies a vortex when the second intermediate eigenvalue of the 3 x 3 tensor A is symmetric (all three eigenvalues are real).

In our original study, the normalized Q and λ_2 values were tested to identify vortices within IAs.

$$Q(x,t) = \frac{Q(x,t)}{|\vec{u}(x,t)|^2}$$
$$\lambda_2(x,t) = \frac{\lambda_2(x,t)}{|\vec{u}(x,t)|^2} \qquad (2.4)$$

Eirmod malorum vis ei. Choro euismod incorrupte in vim, ludus ornatus vis ex. Hinc wisi impedit eum no, vocent definiebas referrentur in quo. Sanctus vulputate repudiandae usu ut. In prima quaeque diceret pri. Enim labores contentiones eos at, duo altera denique nominavi ea, eos inani nominavi consectetuer at.

Liber liberavisse nec at, movet albucius principes has at. Ea sed persius accusam, clita sententiae adversarium ne sed. Usu no graecis theophrastus delicatissimi, sint aliquam an eam. Mei elit mnesarchum dissentias te, in essent laboramus per. Affert mucius quidam mel ex, per dicam insolens ad.

(a) Generic   (b) 200 bins

Figure 2.1: Histogram of nearest neighbors

Docendi eligendi sit et, pri ea dicam eligendi percipitur, has soleat dolores convenire te. Sed altera placerat an, id verterem abhorreant interesset mea. Eum at ceteros efficiantur. Eos id voluptaria efficiendi comprehensam.

In mel modo dicam vocibus, eruditi consectetuer vim no, cu quaestio instructior eum. Justo nostrud fuisset ea mea, eam an libris repudiandae vituperatoribus. Est choro corrumpit definitionem at. Vel sint adhuc vocibus ea, illud epicuri eos no. Sea simul officiis ea, et qui veri invidunt appellantur. Vix et eros ancillae pertinax.

Aliquip lobortis ei est, at error viris graeco sed. Vel te elitr detracto, modo graecis scripserit ex nec. Errem utamur viderer per no, eam ea eripuit referrentur. Pro te dicat disputando.

Table 2.1

A portrait table: first column represents the year in which the Nobel prize in physics was awarded; second column indicates the name of the scientist and the third column is the work for which the Nobel prize was awareded

Year	Scientist(s)	Nobel Work
1901	W. C. Röntgen	X-rays
1902	H. A. Lorentz	Influence of magnetism on radiation
	P. Zeeman	Influence of magnetism on radiation
1903	A. H. Becquerel	Spontaneous radioactivity
	M. Curie	Radiation phenomena discovered by Becquerel
	P. Curie	Radiation phenomena discovered by Becquerel
1904	J. W. Strutt	Argon
1905	P. E. A. von Lenard	Cathode rays
1906	J. J. Thomson	Electrical conductivity of gases
1907	A. A. Michelson	Spectroscopic and metrological investigations
1908	G. Lippmann	Photographic reproduction of colours
1909	K. F. Braun	Wireless telegraphy
	G. Marconi	Wireless telegraphy
1910	J. D. van der Waals	Equation of state of gases and liquids
1911	W. Wien	Laws governing heat radiation
1912	N. G. Dalèn	Automatic regulators for lighting coastal beacons and light buoys

As explained in Table 2.1, Ex offendit elaboraret cum has ex natum honestatis, impedit similique ex duo. Et mei mollis scripta, et vim labores phaedrum, in cum facete saperet. Splendide elaboraret comprehensam qui ne. Putant verterem no vim, mea solum veritus definitiones ei, no labitur propriae deseruisse est. Ius illud everti salutandi id, eu facer pericula principes est.
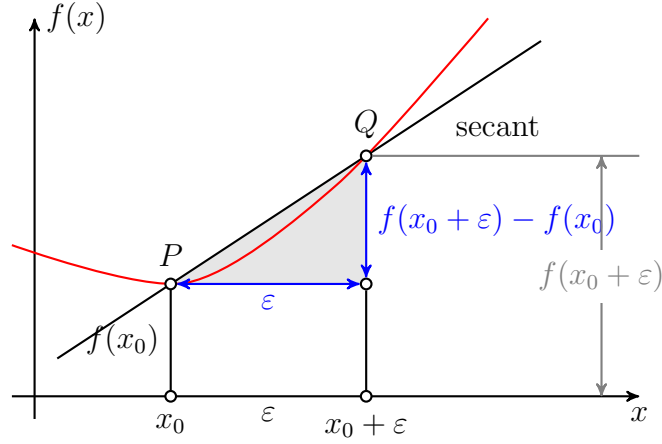
Figure 2.2: Fancy mathematical plots using TikZ package

Simul noster voluptaria eam ei, sint regione pri ei. Cum no utinam equidem, falli bonorum prodesset an qui. Alterum dissentiet vituperatoribus te eam, eos ea suas oblique. Per ea utinam facilisi. Per iudico probatus complectitur et, cum tollit atomorum rationibus ea.
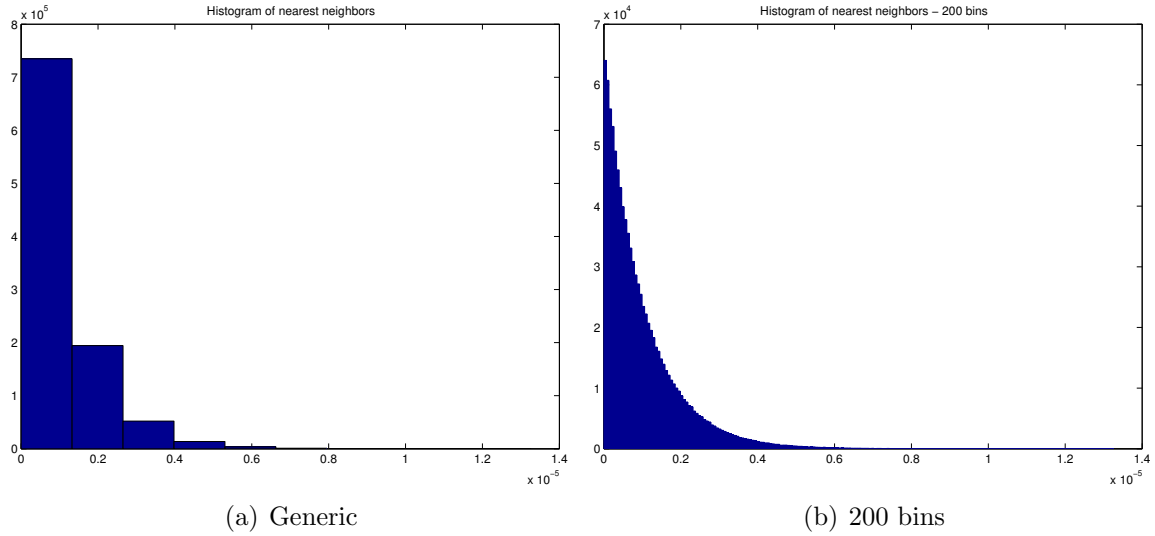
Docendi eligendi sit et, pri ea dicam eligendi percipitur, has soleat dolores convenire te. Sed altera placerat an, id verterem abhorreant interesset mea. Eum at ceteros efficiantur. Eos id voluptaria efficiendi comprehensam.

Simul noster voluptaria eam ei, sint regione pri ei. Cum no utinam equidem, falli bonorum prodesset an qui. Alterum dissentiet vituperatoribus te eam, eos ea suas oblique. Per ea utinam facilisi. Per iudico probatus complectitur et, cum tollit atomorum rationibus ea.

Docendi eligendi sit et, pri ea dicam eligendi percipitur, has soleat dolores convenire

Figure 2.3: Incidence, transmission and reflection

te. Sed altera placerat an, id verterem abhorreant interesset mea. Eum at ceteros efficiantur. Eos id voluptaria efficiendi comprehensam. Simul noster voluptaria eam ei, sint regione pri ei. Cum no utinam equidem, falli bonorum prodesset an qui.

Chapter 3

Vortex Analysis to predict IA Initiation

The tangential, frictional stress caused by blood flowing along the vessel wall is known as WSS. The ANSYS-FLUENT software calculates WSS by the normal velocity gradient at the vessel wall:

$$\tau_{\mathrm{w}} = \mu \frac{\partial v}{\partial n} \tag{3.1}$$

where μ is the dynamic viscosity. In this work, areas of high WSS were of interest as it is thought to play a role in the IA initiation [101]. High WSS was defined as values ≥ 20 Pa during peak systole of the MRI waveform.

The WSSG was calculated using in-house VMTK scripts and is derived from three

spatial derivatives of the WSS as follows:

$$WSSG = \sqrt{(\frac{\partial \tau_w}{\partial x})^2 + (\frac{\partial \tau_w}{\partial y})^2 + (\frac{\partial \tau_w}{\partial z})^2} \qquad (3.2)$$

with the time-averaged WSSG calculated as

$$WSSG_{\text{av}} = \frac{1}{T} \int_0^T |WSSG| dt \qquad (3.3)$$

OSI is a nondimentional parameter, computing oscillations in the direction of the WSS vectors over the course of a cardiac cycle:

$$OSI = \frac{1}{2} \left\{ 1 - \frac{|\int_0^T \tau_i dt|}{\int_0^T |\tau_i| dt} \right\} \qquad (3.4)$$

were τ_i represents the WSS vector at a given time step across the duration of the cardiac cycle (T). The OSI describes the changes of a WSS vector's alignment with the cardiac cycle's temporally-averaged WSS vector. An OSI of 0 indicates no change in directionality and 0.5 being a complete direction reversal.

The AFI [?] quantifies the variation in angle between the instantaneous WSS vector and time-averaged WSS vector:

$$AFI = cos(\theta) = \frac{\tau_i \cdot \tau_{av}}{|\tau_i| * |\tau_{av}|} \qquad (3.5)$$

For each point along the vessel wall, the minimum AFI calculated during the cardiac cycle was used to indicate the greatest deviation of the WSS vector from its mean direction. A minimum AFI of -1, 0, and 1 indicate deviations of 180°, 90°, and 0°respectively.

The GON index [**?**] quantifies fluctuations in WSSG directionality over the cardiac cycle.

$$GON = 1 - \frac{|\int_0^T G dt|}{\int_0^T |G| dt} \tag{3.6}$$

T is the period of the cardiac cycle and G is the spatial wall shear stress gradient vector

Lorem ipsum dolor sit amet, at qui viderer recusabo aliquando, dignissim evertitur ei his. Ignota iuvaret fabulas ei vim. Ne utinam inciderint quo. Pri ea congue postulant conclusionemque. In prima quaeque diceret pri. Enim labores contentiones eos at, duo altera denique nominavi ea, eos inani nominavi consectetuer at. Ut elitr dicam elaboraret pro, ius altera voluptaria cu.

Discere dissentiet vel et, soluta nostrum epicurei ad eam, cu has aperiam vituperata. In prima quaeque diceret pri. Enim labores contentiones eos at, duo altera denique nominavi ea, eos inani nominavi consectetuer at. Ut elitr dicam elaboraret pro, ius altera voluptaria cu. Eam mazim aliquip cu, recusabo pericula accommodare at mea, facer affert nonumes qui ea. [3, 50]

$$d\nu_\theta \; = \; \frac{N}{V} \left(\frac{m}{2\pi \, kT}\right)^{3/2} \left[\int_0^{2\pi} \int_0^\infty v^3 \, e^{-mv^2/2kT} \, dv \, d\phi\right] \sin\theta \; \cos\theta \; d\theta$$

$$= \; 2\,\pi \, \frac{N}{V} \left(\frac{m}{2\pi \, kT}\right)^{3/2} \left[\int_0^\infty v^3 \, e^{-mv^2/2kT} \, dv\right] \sin\theta \; \cos\theta \; d\theta$$

At vix indoctum disputando. Eam cu doctus reprimique, quaeque democritum an eos, sit veniam facete dissentias id. Tale volumus eos te, an eum nulla tincidunt. Mea id recteque theophrastus.

$$d\nu_\theta \; = \; \frac{N}{V} \left(\frac{2\,k\,T}{m\,\pi}\right)^{1/2} \sin\theta \; \cos\theta \; d\theta \qquad\qquad (3.7)$$

Liber liberavisse nec at, movet albucius principes has at. Ea sed persius accusam, clita sententiae adversarium ne sed. Usu no graecis theophrastus delicatissimi, sint aliquam an eam. Mei elit mnesarchum dissentias te, in essent laboramus per. Affert mucius quidam mel ex, per dicam insolens ad.

Sed altera placerat an, id verterem abhorreant interesset mea. Eum at ceteros efficiantur. Eos id voluptaria efficiendi comprehensam. Continuing from Eqn. (3.7)

$$dv_v = \frac{N}{V} \left(\frac{m}{2\pi\,kT}\right)^{3/2} \left[\int_0^{2\pi} \int_0^{\pi/2} \sin\theta\,\cos\theta\,d\theta\,d\phi\right] v^3\,e^{-mv^2/2kT}\,dv$$

$$= 2\,\pi\,\frac{N}{V}\,\left(\frac{m}{2\pi\,kT}\right)^{3/2} \left[\int_0^{\pi/2} \sin\theta\,\cos\theta\,d\theta\right] v^3\,e^{-mv^2/2kT}\,dv$$

In mel modo dicam vocibus, eruditi consectetuer vim no, cu quaestio instructior eum. Justo nostrud fuisset ea mea, eam an libris repudiandae vituperatoribus. Est choro corrumpit definitionem at. Vel sint adhuc vocibus ea, illud epicuri eos no. Sea simul officiis ea, et qui veri invidunt appellantur. Vix et eros ancillae pertinax.

In mel modo dicam vocibus, eruditi consectetuer vim no, cu quaestio instructior eum. Justo nostrud fuisset ea mea, eam an libris repudiandae vituperatoribus. Est choro corrumpit definitionem at. Vel sint adhuc vocibus ea, illud epicuri eos no. Sea simul officiis ea, et qui veri invidunt appellantur. Vix et eros ancillae pertinax.

$$dv_v = \frac{N}{V}\,\pi\,\left(\frac{m}{2\pi\,kT}\right)^{3/2} v^3\,e^{-mv^2/2kT}\,dv \tag{3.8}$$

Aliquip lobortis ei est, at error viris graeco sed. Vel te elitr detracto, modo graecis scripserit ex nec. Errem utamur viderer per no, eam ea eripuit referrentur. Pro te dicat disputando.
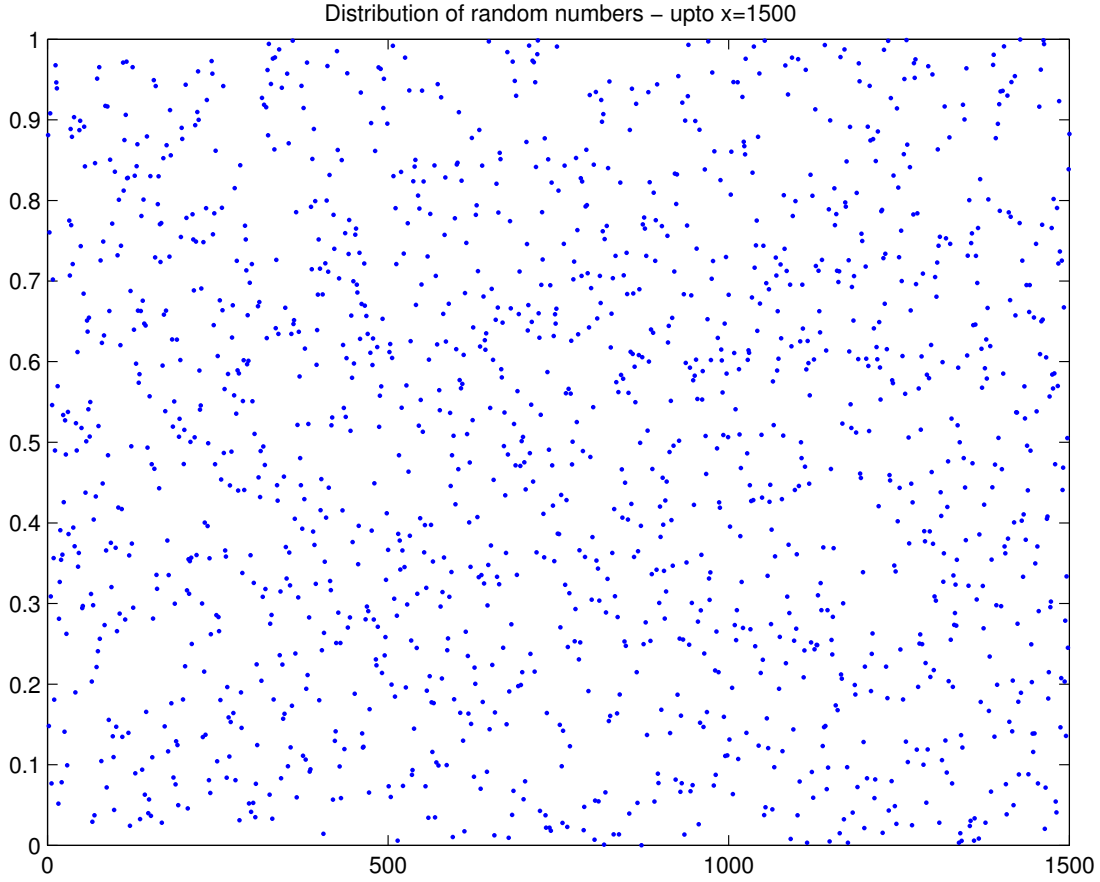
Figure 3.1: Distribution of random numbers

Table 3.1

Measured data points representing the relationship between x and y

x	0	1	2	3	4	5	6	7	8	9	10
y	0	0.94	0.99	-0.52	-1.82	-0.44	3.54	6.69	5.38	0.00	-4.42

Et mei mollis scripta, et vim labores phaedrum, in cum facete saperet. Splendide elaboraret comprehensam qui ne. Putant verterem no vim, mea solum veritus definitiones ei, no labitur propriae deseruisse est. Ius illud everti salutandi id, eu facer pericula principes est.

Table 3.2

A landscape table: first column represents the year in which the Nobel
prize in physics was awarded; second column indicates the name of the
scientist and the third column is an *as is* Nobel citation

Year	Scientist(s)	Nobel Work
1901	W. C. Röntgen	in recognition of the extraordinary services he has rendered by the discovery of the remarkable rays subsequently named after him
1902	H. A. Lorentz and P. Zeeman	in recognition of the extraordinary service they rendered by their researches into the influence of magnetism upon radiation phenomena
1903	A. H. Becquerel	in recognition of the extraordinary services he has rendered by his discovery of spontaneous radioactivity
	M. Curie and P. Curie	in recognition of the extraordinary services they have rendered by their joint researches on the radiation phenomena discovered by Prof. Henri Becquerel
1904	J. W. Strutt	for his investigations of the densities of the most important gases and for his discover argon in connection with these studies
1905	P. E. A. von Lenard	Cathode rays
1906	J. J. Thomson	Electrical conductivity of gases
1907	A. A. Michelson	Spectroscopic and metrological investigations
1908	G. Lippmann	Photographic reproduction of colours
1909	K. F. Braun and G. Marconi	Wireless telegraphy
1910	J. D. van der Waals	Equation of state of gases and liquids
1911	W. Wien	Laws governing heat radiation
1912	N. G. Dalèn	Automatic regulators for lighting coastal beacons and light buoys

Et mei mollis scripta, et vim labores phaedrum, in cum facete saperet. Splendide elaboraret comprehensam qui ne. Putant verterem no vim, mea solum veritus definitiones ei, no labitur propriae deseruisse est. Ius illud everti salutandi id, eu facer pericula principes est.
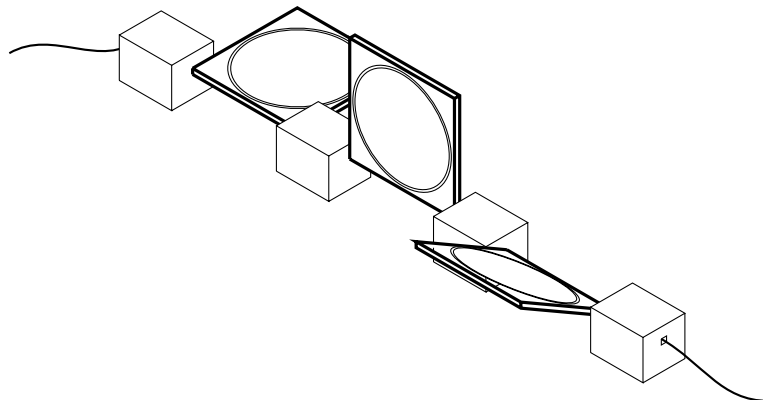
Figure 3.2: Fibre optics

Simul noster voluptaria eam ei, sint regione pri ei. Cum no utinam equidem, falli bonorum prodesset an qui. Alterum dissentiet vituperatoribus te eam, eos ea suas oblique. Per ea utinam facilisi. Docendi eligendi sit et, pri ea dicam eligendi percipitur, has soleat dolores convenire te.

Adipisci molestiae vim at, eum everti accommodare eu. Duo ex maiorum consetetur. Sea et vivendo concludaturque, rebum conclusionemque pro eu. Mei an everti dolorem. Per id alterum mandamus deseruisse. Copiosae evertitur eum ea, atqui interesset est in. Vim magna munere nostrum an, cu congue equidem est. Mediocrem reformidans ne mel. Et summo nihil mel, an nam postea incorrupte.

In amet verear evertitur qui, ex mea vivendo hendrerit. Ad posse perfecto prodesset usu, cum fugit accumsan no. Tempor nonumes duo ea, oblique fabulas salutatus ne vis. Ne eam scripta dolorem, graece eruditi eum ei. Ei sed brute zril nostro, nostro voluptatum id sea, courtesy of Wikipedia. [67] Adipisci molestiae vim at, eum everti accommodare eu. Duo ex maiorum consetetur. Sea et vivendo concludaturque, rebum conclusionemque pro eu.

Adipisci molestiae vim at, eum everti accommodare eu. Duo ex maiorum consetetur. Sea et vivendo concludaturque, rebum conclusionemque pro eu. Mei an everti dolorem. Per id alterum mandamus deseruisse. Copiosae evertitur eum ea, atqui interesset est in. Vim magna munere nostrum an, cu congue equidem est. Mediocrem reformidans ne mel. Et summo nihil mel, an nam postea incorrupte an everti dolorem. Per id alterum mandamus deseruisse. Copiosae evertitur eum ea, atqui interesset est in. Vim magna munere nostrum an, cu congue equidem est. Mediocrem reformidans ne mel. Et summo nihil mel, an nam postea incorrupte. Mediocrem reformidans ne mel. Et summo nihil mel, an nam postea incorrupte an everti dolorem.

Per id alterum mandamus deseruisse. Copiosae evertitur eum ea, atqui interesset est in. Vim magna munere nostrum an, cu congue equidem est. Mediocrem reformidans ne mel. Et summo nihil mel, an nam postea incorrupte.
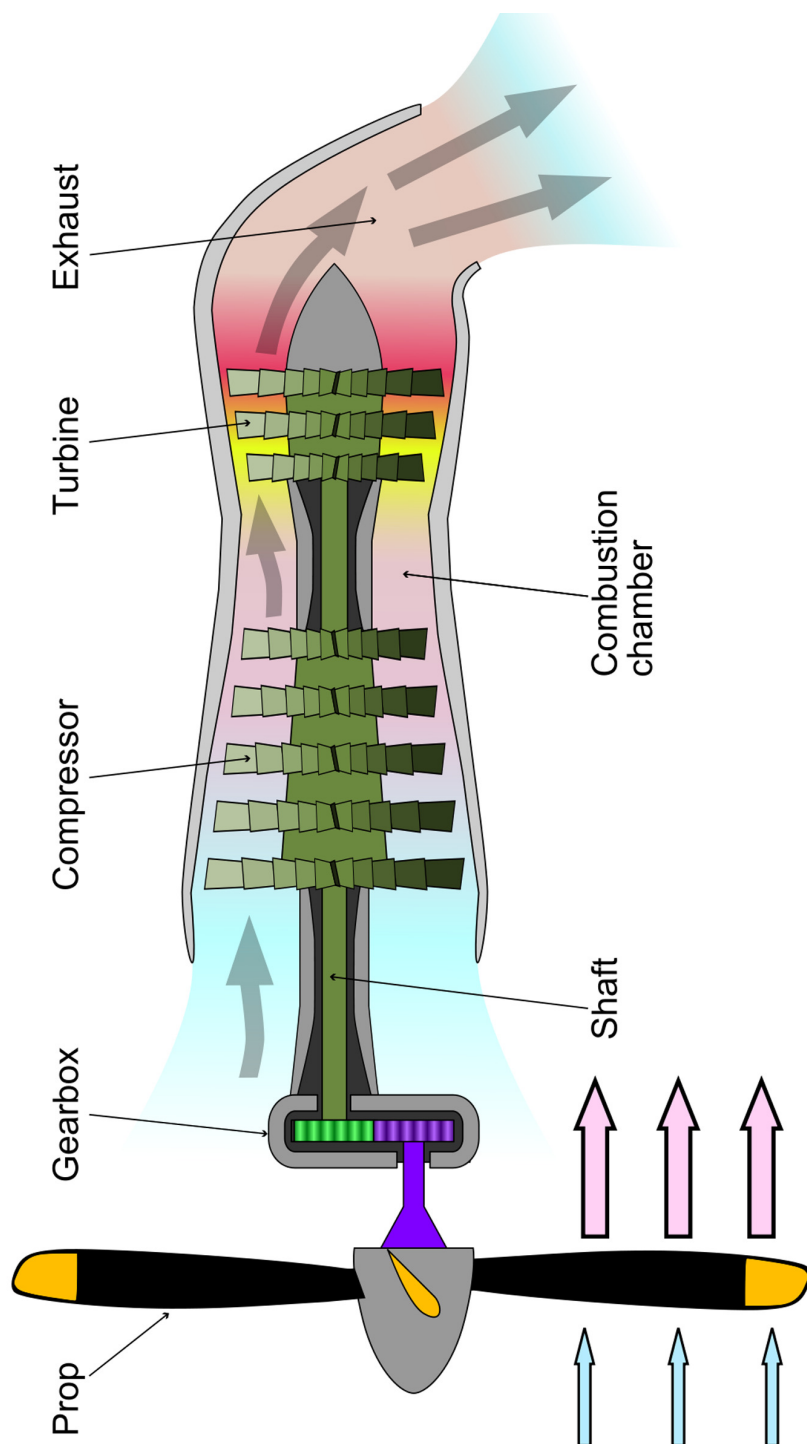
Figure 3.3: A landscape view of a Turboprop engine - these are jet engine derivatives, still gas turbines, that extract work from the hot-exhaust jet to turn a rotating shaft, which is then used to produce thrust by some other means

Id ius soluta semper audiam, ad eos scriptorem concludaturque, id mel rebum volumus deserunt. Mel libris percipit scriptorem te, his an dicat putent menandri, mazim officiis aliquando mei no. Ne clita veniam disputando vim, postea hendrerit maiestatis qui id. Mei te suscipit quaerendum, an aliquando intellegebat ius, ei simul detraxit dissentiet eam. Zril dolor ut usu.

Everti saperet vis ut. Scripta maluisset mel eu, duis antiopam in pro. Sea diceret contentiones ea. Nec eu duis efficiantur, evertitur constituam mediocritatem te vis, pro error regione ad. Sit malorum aliquam at, pericula dissentias mei ei. Cu soluta urbanitas est, albucius vituperatoribus usu et.

References

[1] ABBOUD, T., RUSTOM, J., BESTER, M., CZORLICH, P., VITTORAZZI, E., PINNSCHMIDT, H. O., WESTPHAL, M., AND REGELSBERGER, J. Morphology of ruptured and unruptured intracranial aneurysms. *World neurosurgery 99* (2017), 610–617.

[2] AIRD, W. Spatial and temporal dynamics of the endothelium. *Journal of Thrombosis and Haemostasis 3*, 7 (2005), 1392–1406.

[3] ANDERSON, E., BAI, Z., BISCHOF, C., BLACKFORD, S., DEMMEL, J., DONGARRA, J. J., CROZ, J. D., GREENBAUM, A., HAMMARLING, S., MCKENNEY, A., AND SORENSEN, D. *LAPACK Users' Guide*, 3 ed. Society for Industrial and Applied Mathematics, Philadelphia, PA, 1999.

[4] ANTIGA, L., AND STEINMAN, D. A. Robust and objective decomposition and mapping of bifurcating vessels. *IEEE transactions on medical imaging 23*, 6 (2004), 704–713.

[5] AOKI, T., YAMAMOTO, K., FUKUDA, M., SHIMOGONYA, Y., FUKUDA, S., AND NARUMIYA, S. Sustained expression of mcp-1 by low wall shear stress loading concomitant with turbulent flow on endothelial cells of intracranial aneurysm. *Acta Neuropathologica Communications 4*, 1 (2016), 48.

[6] BACKES, D., RINKEL, G. J., LABAN, K. G., ALGRA, A., AND VERGOUWEN, M. D. Patient- and aneurysm-specific risk factors for intracranial aneurysm growth. *Stroke 47*, 4 (2016), 951–957.

[7] BAEK, H., JAYARAMAN, M., RICHARDSON, P., AND KARNIADAKIS, G. Flow instability and wall shear stress variation in intracranial aneurysms. *Journal of the Royal Society Interface* (2009), rsif20090476.

[8] BALAGURU, U. M., SUNDARESAN, L., MANIVANNAN, J., MAJUNATHAN, R., MANI, K., SWAMINATHAN, A., VENKATESAN, S., KASIVISWANATHAN, D., AND CHATTERJEE, S. Disturbed flow mediated modulation of shear forces on endothelial plane: A proposed model for studying endothelium around atherosclerotic plaques. *Scientific reports 6* (2016), 27304.

[9] BARATCHI, S., KHOSHMANESH, K., WOODMAN, O. L., POTOCNIK, S., PETER, K., AND MCINTYRE, P. Molecular sensors of blood flow in endothelial cells. *Trends in molecular medicine 23*, 9 (2017), 850–868.

[10] BARÁTH, K., CASSOT, F., RÜFENACHT, D. A., AND FASEL, J. H. Anatomically shaped internal carotid artery aneurysm in vitro model for flow analysis

to evaluate stent effect. *American Journal of Neuroradiology 25*, 10 (2004), 1750–1759.

[11] BAZILEVS, Y., HSU, M.-C., ZHANG, Y., WANG, W., KVAMSDAL, T., HENTSCHEL, S., AND ISAKSEN, J. Computational vascular fluid–structure interaction: methodology and application to cerebral aneurysms. *Biomechanics and modeling in mechanobiology 9*, 4 (2010), 481–498.

[12] BIASETTI, J., HUSSAIN, F., AND GASSER, T. C. Blood flow and coherent vortices in the normal and aneurysmatic aortas: a fluid dynamical approach to intra-luminal thrombus formation. *Journal of The Royal Society Interface* (2011), rsif20110041.

[13] BRINJIKJI, W., ZHU, Y.-Q., LANZINO, G., CLOFT, H., MURAD, M., WANG, Z., AND KALLMES, D. Risk factors for growth of intracranial aneurysms: A systematic review and meta-analysis. *American Journal of Neuroradiology* (2015).

[14] BYRNE, G., AND CEBRAL, J. Vortex dynamics in cerebral aneurysms. *arXiv preprint arXiv:1309.7875* (2013).

[15] BYRNE, G., MUT, F., AND CEBRAL, J. Quantifying the large-scale hemodynamics of intracranial aneurysms. *American Journal of Neuroradiology 35*, 2 (2014), 333–338.

[16] CAN, A., AND DU, R. Association of hemodynamic factors with intracranial aneurysm formation and rupture: systematic review and meta-analysis. *Neurosurgery 78*, 4 (2015), 510–520.

[17] CAR, R., AND PARRINELLO, M. Unified Approach for Molecular Dynamics and Density-Functional Theory. *Physical Review Letters 55* (1985), 2471.

[18] CASTRO, M. A., OLIVARES, M. C. A., PUTMAN, C. M., AND CEBRAL, J. R. Wall motion and hemodynamics in intracranial aneurysms. In *Journal of Physics: Conference Series* (2013), vol. 477, IOP Publishing, p. 012004.

[19] CEBRAL, J., OLLIKAINEN, E., CHUNG, B. J., MUT, F., SIPPOLA, V., JAHROMI, B. R., TULAMO, R., HERNESNIEMI, J., NIEMELÄ, M., ROBERTSON, A., AND FRÖSEN, J. Flow conditions in the intracranial aneurysm lumen are associated with inflammation and degenerative changes of the aneurysm wall. *American Journal of Neuroradiology 38*, 1 (2017), 119–126.

[20] CECCHI, E., GIGLIOLI, C., VALENTE, S., LAZZERI, C., GENSINI, G. F., ABBATE, R., AND MANNINI, L. Role of hemodynamic shear stress in cardiovascular disease. *Atherosclerosis 214*, 2 (2011), 249–256.

[21] CHALOUHI, N., HOH, B. L., AND HASAN, D. Review of cerebral aneurysm formation, growth, and rupture. *Stroke 44*, 12 (2013), 3613–3622.

[22] CHALOUHI, N., ZANATY, M., WHITING, A., YANG, S., TJOUMAKARIS, S., HASAN, D., STARKE, R. M., HANN, S., HAMMER, C., KUNG, D., AND

ET. AL. Safety and efficacy of the pipeline embolization device in 100 small intracranial aneurysms. *Journal of neurosurgery 122*, 6 (2015), 1498–1502.

[23] CHEN, C.-N., CHANG, S.-F., LEE, P.-L., CHANG, K., CHEN, L.-J., USAMI, S., CHIEN, S., AND CHIU, J.-J. Neutrophils, lymphocytes, and monocytes exhibit diverse behaviors in transendothelial and subendothelial migrations under coculture with smooth muscle cells in disturbed flow. *Blood 107*, 5 (2006), 1933–1942.

[24] CHEN, Z., AND TZIMA, E. Pecam-1 is necessary for flow-induced vascular remodeling. *Arteriosclerosis, thrombosis, and vascular biology 29*, 7 (2009), 1067–1073.

[25] CHIEN, S. Mechanotransduction and endothelial cell homeostasis: the wisdom of the cell. *American Journal of Physiology-Heart and Circulatory Physiology 292*, 3 (2007), H1209–H1224.

[26] CHIU, J.-J., AND CHIEN, S. Effects of disturbed flow on vascular endothelium: pathophysiological basis and clinical perspectives. *Physiological reviews 91*, 1 (2011), 327–387.

[27] THE CPMD CONSORTIUM. *CPMD (v3.15.1): An ab initio Electronic Structure and Molecular Dynamcis Program*, 2011.

[28] DELLEY, B. An All-Electron Numerical Method for Solving the Local Density Functional for Polyatomic Molecules. *Journal of Chemical Physics 92* (1990), 508.

[29] DELLEY, B. Fast Calculation of Electrostatics in Crystals and Large Molecules. *Journal of Physical Chemistry 100* (1996), 6107.

[30] DEMARTINI, L. C., VIELMO, H. A., AND MÖLLER, S. Numeric and experimental analysis of the turbulent flow through a channel with baffle plates. *Journal of the Brazilian Society of Mechanical Sciences and Engineering 26*, 2 (2004), 153–159.

[31] DEMPERE-MARCO, L., OUBEL, E., CASTRO, M., PUTMAN, C., FRANGI, A., AND CEBRAL, J. Cfd analysis incorporating the influence of wall motion: application to intracranial aneurysms. In *International Conference on Medical Image Computing and Computer-Assisted Intervention* (2006), Springer, pp. 438–445.

[32] DEPLANO, V., KNAPP, Y., BERTRAND, E., AND GAILLARD, E. Flow behaviour in an asymmetric compliant experimental model for abdominal aortic aneurysm. *Journal of biomechanics 40*, 11 (2007), 2406–2413.

[33] DOLAN, J. M., KOLEGA, J., AND MENG, H. High wall shear stress and spatial gradients in vascular pathology: a review. *Annals of biomedical engineering 41*, 7 (2013), 1411–1427.

[34] DOLAN, J. M., MENG, H., SINGH, S., PALUCH, R., AND KOLEGA, J. High fluid shear stress and spatial shear stress gradients affect endothelial proliferation, survival, and alignment. *Annals of biomedical engineering 39*, 6 (2011), 1620–1631.

[35] DONGARRA, J. J. LINPACK Working Note 3: Fortran BLAS Timing. *Argonne National Laboratory Report, ANL-80-24* (1980).

[36] DONGARRA, J. J., BUNCH, J., MOLER, C., AND STEWART, G. W. *LINPACK User's Guide*. Society for Industrial and Applied Mathematics, Philadelphia, PA, 1979.

[37] DONGARRA, J. J., CROZ, J. D., HAMMARLING, S., AND DUFF, I. S. A Set of Level 3 Basic Linear Algebra Subprograms. *Association for Computing Machinery Transactions on Mathematical Software 16* (1990), 1.

[38] DONGARRA, J. J., CROZ, J. D., HAMMARLING, S., AND HANSON, R. An Extended Set of FORTRAN Basic Linear Algebra Subprograms. *Association for Computing Machinery Transactions on Mathematical Software 14* (1988), 1.

[39] DOVESI, R., ORLANDO, R., CIVALLERI, B., ROETTI, C., SAUNDERS, V. R., AND ZICOVICH-WILSON, C. M. CRYSTAL: A Computational Tool for the Ab Initio Study of the Electronic Properties of Crystals. *Zieitschrift für Kristallographie 220* (2005), 571.

[40] Dovesi, R., Saunders, V. R., Roetti, C., Orlando, R., Zicovich-Wilson, C. M., Pascale, F., Civalleri, B., Doll, K., Harrison, N. M., Bush, I. J., D'Arco, P., and Llunell, M. *CRYSTAL 09 User's Manual.* University of Torino, Italy, 2009.

[41] Duan, Z., Li, Y., Guan, S., Ma, C., Han, Y., Ren, X., We, L., Li, W., Lo, J., and Yang, Z. Morphological parameters and anatomical locations associated with rupture status of small intracranial aneurysms. *Scientific reports 8* (2018).

[42] Efron, B., Hastie, T., Johnstone, I., Tibshirani, R., and et. al. Least angle regression. *The Annals of statistics 32*, 2 (2004), 407–499.

[43] Elad, D., and Einav, S. Physical and flow properties of blood. *Standard handbook of biomedical engineering and design* (2004), 3–1.

[44] Etminan, N., Brown, R. D., Beseoglu, K., Juvela, S., Raymond, J., Morita, A., Torner, J. C., Derdeyn, C. P., Raabe, A., Mocco, J., and et. al. The unruptured intracranial aneurysm treatment score a multidisciplinary consensus. *Neurology 85*, 10 (2015), 881–889.

[45] Falgout, R. D., and Yang, U. M. HYPRE: A Library of High Performance Preconditioners. In *Proceedings of the International Conference on Computational Science - Part III* (London, UK, 2002), ICCS '02, Springer-Verlag, p. 632.

[46] FELICIANI, G., POTTERS, W. V., VAN OOIJ, P., SCHNEIDERS, J. J., NEDERVEEN, A. J., VAN BAVEL, E., MAJOIE, C. B., AND MARQUERING, H. A. Multiscale 3-d+ t intracranial aneurysmal flow vortex detection. *IEEE Trans. Biomed. Engineering 62*, 5 (2015), 1355–1362.

[47] FORD, M., HOI, Y., PICCINELLI, M., ANTIGA, L., AND STEINMAN, D. An objective approach to digital removal of saccular aneurysms: technique and applications. *The British Journal of Radiology 82*, special_issue_1 (2009), S55–S61.

[48] FORD, M. D., ALPERIN, N., LEE, S. H., HOLDSWORTH, D. W., AND STEINMAN, D. A. Characterization of volumetric flow rate waveforms in the normal internal carotid and vertebral arteries. *Physiological measurement 26*, 4 (2005), 477.

[49] FORD, M. D., NIKOLOV, H. N., MILNER, J. S., LOWNIE, S. P., DEMONT, E. M., KALATA, W., LOTH, F., HOLDSWORTH, D. W., AND STEINMAN, D. A. Piv-measured versus cfd-predicted flow dynamics in anatomically realistic cerebral aneurysm models. *Journal of biomechanical engineering 130*, 2 (2008), 021015.

[50] FRIGO, M., AND JOHNSON, S. G. The Design and Implementation of FFTW3. In *Proceedings of the IEEE* (2005), vol. 93, p. 216.

[51] Fung, J. C. H. Residence time of inertial particles in a vortex. *Journal of Geophysical Research: Oceans 105*, C6 (2000), 14261–14272.

[52] Gabriel, S. A., Ding, Y., and Feng, Y. Quantifying the influence of oscillatory flow disturbances on blood flow. *Journal of Theoretical Biology 430* (2017), 195 – 206.

[53] Gale, J. D. Empirical Potential Derivation for Ionic Materials. *Philosophical Magazine B 73* (1996), 3.

[54] Gale, J. D. GULP - A Computer Program for the Symmetry Adapted Simulation of Solids. *Journal of Chemical Society, Faraday Transactions 93* (1997), 629.

[55] Greving, J. P., Wermer, M. J., Jr, M. J. B., Morit, A., Juvela, S., Yonekura, M., Ishibashi, T., Torner, J. C., Nakayama, T., Rinkel, G. J., and et. al. Development of the phases score for prediction of risk of rupture of intracranial aneurysms: a pooled analysis of six prospective cohort studies. *The Lancet Neurology 13*, 1 (2014), 59–66.

[56] gsam Kim, Y., Par, Y., and Lim, S. 3d simulations of blood flow dynamics in compliant vessels: normal, aneurysmal, and stenotic arteries. *Communications in Computational Physics 19*, 5 (2016), 1167–1190.

[57] Hackenberg, K. A., Hänggi, D., and Etminan, N. Unruptured intracranial aneurysms: Contemporary data and management. *Stroke 49*, 9 (2018), 2268–2275.

[58] Haimes, R., and Kenwright, D. On the velocity gradient tensor and fluid feature extraction. In *14th Computational Fluid Dynamics Conference* (1999), p. 3288.

[59] Hanczar, B., Hu, J., Sim, C., Weinstein, J., Bittner, M., and RDougherty, E. Small-sample precision of roc-related estimates. *Bioinformatics 26*, 6 (2010), 822–830.

[60] Hanley, J. A., and McNeil, B. J. The meaning and use of the area under a receiver operating characteristic (roc) curve. *Radiology 143*, 1 (1982), 29–36.

[61] Harrell, F. E., Lee, K. L., and Mark, D. B. Multivariable prognostic models: issues in developing models, evaluating assumptions and adequacy, and measuring and reducing errors. *Statistics in medicine 15*, 4 (1996), 361–387.

[62] Hasan, D. M., Nadareyshvili, A. I., Hoppe, A. L., Mahane, K. B., Kung, D. K., and Raghavan, M. L. Cerebral aneurysm sac growth as the etiology of recurrence after successful coil embolization. *Stroke 43*, 3 (2012), 866–868.

[63] Helmke, B. P. Molecular control of cytoskeletal mechanics by hemodynamic forces. *Physiology 20*, 1 (2005), 43–53.

[64] HESS, B., KUTZNER, C., VAN DER SPOEL, D., AND LINDAHL, E. GROMACS 4: Algorithms for Highly Efficient, Load-Balanced, and Scalable Molecular Simulation. *Journal of Chemical Theory and Computation 4* (2008), 235.

[65] HOLDSWORTH, D., NORLEY, C., FRAYNE, R., STEINMAN, D., AND RUTT, B. Characterization of common carotid artery blood-flow waveforms in normal human subjects. *Physiological measurement 20*, 3 (1999), 219.

[66] HOPPE, A. L., RAGHAVA, M. L., AND HASAN, D. M. Comparison of the association of sac growth and coil compaction with recurrence in coil embolized cerebral aneurysms. *PloS one 10*, 4 (2015), e0123017.

[67] HTTP://WIKIPEDIA.ORG/. *Wikipedia.* Wikipedia, The Internet, 2012.

[68] HUMPHREY, W., DALKE, A., AND SCHULTEN, K. VMD - Visual Molecular Dynamics. *Journal of Molecular Graphics 14* (1996), 33.

[69] HUNT, J. C., WRAY, A. A., AND MOIN, P. Eddies, streams, and convergence zones in turbulent flows.

[70] HUO, Y., CHOY, J. S., SVENDSEN, M., SINHA, A. K., AND KASSAB, G. S. Effects of vessel compliance on flow pattern in porcine epicardial right coronary arterial tree. *Journal of biomechanics 42*, 5 (2009), 594–602.

[71] ILDIKO, F. E., AND FRIEDMAN, J. H. A statistical view of some chemometrics regression tools. *Technometrics 35*, 2 (1993), 109–135.

[72] JEONG, J., AND HUSSAIN, F. On the identification of a vortex. *Journal of fluid mechanics 285* (1995), 69–94.

[73] JIANG, M., MACHIRAJU, R., AND THOMPSON, D. Detection and visualization of vortices. *The visualization handbook 295* (2005).

[74] JR, T. R. F., BENITEZ, R., VEZNEDAROGLU, E., SHARAN, A., MITCHELL, W., SILVA, M., AND ROSENWASSER, R. H. A review of size and location of ruptured intracranial aneurysms. *Neurosurgery 49*, 6 (2001), 1322–1326.

[75] JUVELA, S. Risk factors for multiple intracranial aneurysms. *Stroke 31*, 2 (2000), 392–397.

[76] JUVELA, S., POUSSA, K., LEHTO, H., AND PORRAS, M. Natural history of unruptured intracranial aneurysms: a long-term follow-up study. *Stroke 44*, 9 (2013), 2414–2421.

[77] KARINO, T., AND GOLDSMITH, H. Flow behaviour of blood cells and rigid spheres in an annular vortex. *Phil. Trans. R. Soc. Lond. B 279*, 967 (1977), 413–445.

[78] KASHIWAZAKI, D., AND KURODA, S. Size ratio can highly predict rupture risk in intracranial small (¡ 5 mm) aneurysms. *Stroke 44*, 8 (2013), 2169–2173.

[79] KHAN, M., VALEN-SENDSTAD, K., AND STEINMAN, D. Narrowing the expertise gap for predicting intracranial aneurysm hemodynamics: impact of solver

numerics versus mesh and time-step resolution. *American Journal of Neuroradiology* (2015).

[80] KIM, M.-C., NAM, J. H., AND LEE, C.-S. Near-wall deposition probability of blood elements as a new hemodynamic wall parameter. *Annals of Biomedical Engineering 34*, 6 (Jun 2006), 958–970.

[81] KÖHLER, B., GASTEIGER, R., PREIM, U., THEISEL, H., GUTBERLET, M., AND PREIM, B. Semi-automatic vortex extraction in 4d pc-mri cardiac blood flow data using line predicates. *IEEE Transactions on Visualization and Computer Graphics 19*, 12 (2013), 2773–2782.

[82] KOLÁŘ, V. Vortex identification: New requirements and limitations. *International journal of heat and fluid flow 28*, 4 (2007), 638–652.

[83] KOLKAJI, A. *Molecular Graphics Modelling 17* (1999), 176.

[84] KOMOTAR, R. J., MOCCO, J., AND SOLOMON, R. A. Guidelines for the surgical treatment of unruptured intracranial aneurysms: the first annual j. lawrence pool memorial research symposiumcontroversies in the management of cerebral aneurysms. *Neurosurgery 62*, 1 (2008), 183–194.

[85] KORJA, M., LEHTO, H., AND JUVELA, S. Lifelong rupture risk of intracranial aneurysms depends on risk factors. *Stroke 45*, 7 (2014), 1958–1963.

[86] KOTOWSKI, M., NAGGARA, O., DARSAUT, T. E., NOLET, S., GEVRY, G., KOUZNETSOV, E., AND RAYMOND, J. Safety and occlusion rates of surgical treatment of unruptured intracranial aneurysms: a systematic review and meta-analysis of the literature from 1990 to 2011. *Journal of Neurology, Neurosurgery & Psychiatry 84*, 1 (2013), 42–48.

[87] KRESSE, G., AND HAFNER, J. Ab Initio Molecular Dynamics for Liquid Metals. *Physical Review B 47* (1993), 558.

[88] KRESSE, G., AND HAFNER, J. Ab Initio Molecular-Dynamics Simulation of the Liquid-Metal-Amorphous-Semiconductor Transition in Germanium. *Physical Review B 49* (1994), 14251.

[89] KU, D., GIDDENS, D. P., ZARINS, C. K., AND GLAGOV, S. Pulsatile flow and atherosclerosis in the human carotid bifurcation. positive correlation between plaque location and low oscillating shear stress. *Arteriosclerosis: An Official Journal of the American Heart Association, Inc. 5*, 3 (1985), 293–302.

[90] KULCSÁR, Z., UGRON, A., BERENTEI, Z., PAÁL, G., SZIKORA, I., AND ET AL. Hemodynamics of cerebral aneurysm initiation: the role of wall shear stress and spatial wall shear stress gradient. *American Journal of neuroradiology* (2011).

[91] LEE, G., EOM, K., LEE, C., KIM, D., AND KANG, S. Rupture of very small intracranial aneurysms: Incidence and clinical characteristics. *J Cerebrovasc Endovasc Neurosurg 17(3)* (2015), 217–222.

[92] LIU, J., JING, L., WANG, C., ZHANG, Y., AND YANG, X. Recanalization, regrowth, and delayed rupture of a previously coiled unruptured anterior communicating artery aneurysm: a longitudinal hemodynamic analysis. *World neurosurgery 89* (2016), 726–e5.

[93] LIU, X., SUN, A., FAN, Y., AND DENG, X. Physiological significance of helical flow in the arterial system and its potential clinical applications. *Annals of Biomedical Engineering 43*, 1 (Jan 2015), 3–15.

[94] LONGO, M., GRANATA, F., RACCHIUSA, S., MORMINA, E., GRASSO, G., LONGO, G. M., GARUFI, G., SALPIETRO, F. M., AND ALAFACI, C. Role of hemodynamic forces in unruptured intracranial aneurysms: An overview of a complex scenario. *World Neurosurgery 105* (2017), 632 – 642.

[95] LORENSEN, W. E., AND CLINE, H. E. Marching cubes: A high resolution 3d surface construction algorithm. In *ACM siggraph computer graphics* (1987), vol. 21, ACM, pp. 163–169.

[96] MA, D., TREMMEL, M., PALUCH, R. A., LEVY, E. L. I., MENG, H., AND MOCCO, J. Size ratio for clinical assessment of intracranial aneurysm rupture risk. *Neurological research 32*, 5 (2010), 482–486.

[97] MA, J., WANG, C., SHENE, C.-K., AND JIANG, J. A graph-based interface for visualanalytics of 3d streamlines and pathlines. *IEEE transactions on visualization and computer graphics 20*, 8 (2014), 1127–1140.

[98] MANNINO, R. G., MYERS, D. R., AHN, B., WANG, Y., ROLLINS, M., GOLE, H., LIN, A. S., GULDBERG, R. E., GIDDENS, D. P., TIMMINS, L. H., AND ET. AL. Do-it-yourself in vitro vasculature that recapitulates in vivo geometries for investigating endothelial-blood cell interactions. *Scientific reports 5* (2015), 12401.

[99] MARKL, M., WEGENT, F., ZECH, T., BAUER, S., STRECKER, C., SCHUMACHER, M., WEILLER, C., HENNIG, J., AND HARLOFF, A. In vivo wall shear stress distribution in the carotid artery: effect of bifurcation geometry, internal carotid artery stenosis, and recanalization therapy. *Circulation: Cardiovascular Imaging 3*, 6 (2010), 647–655.

[100] MASCITELLI, J. R., OERMANN, E. K., LEACY, R. A. D., MOYLE, H., MOCCO, J., AND PATEL, A. B. Predictors of treatment failure following coil embolization of intracranial aneurysms. *Journal of Clinical Neuroscience 22*, 8 (2015), 1275–1281.

[101] MENG, H., TUTINO, V. M., XIANG, J., AND SIDDIQUI, A. High wss or low wss? complex interactions of hemodynamics with intracranial aneurysm initiation, growth, and rupture: Toward a unifying hypothesis. *American Journal of*

Neuroradiology 35, 7 (2014), 1254–1262.

[102] Miura, Y., Ishida, F., Umeda, Y., Tanemura, H., Suzuki, H., Matsushima, S., Shimosaka, S., and Taki, W. Low wall shear stress is independently associated with the rupture status of middle cerebral artery aneurysms. *Stroke 44*, 2 (2013), 519–521.

[103] Nobari, S., Mongrain, R., Leask, R., and Cartier, R. The effect of aortic wall and aortic leaflet stiffening on coronary hemodynamic: a fluid–structure interaction study. *Medical & biological engineering & computing 51*, 8 (2013), 923–936.

[104] Nowicki, K. W., Hosaka, K., He, Y., McFetridge, P. S., Scott, E. W., and Hoh, B. L. Novel high-throughput in vitro model for identifying hemodynamic-induced inflammatory mediators of cerebral aneurysm formation. *Hypertension 64*, 6 (2014), 1306–1313.

[105] Oeltze-Jafra, S., Cebral, J. R., Janig, G., and Preim, B. Cluster analysis of vortical flow in simulations of cerebral aneurysm hemodynamics. *IEEE transactions on visualization and computer graphics 22*, 1 (2016), 757–766.

[106] Ollikainen, E., Tulamo, R., Lehti, S., Lee-Rueckert, M., Hernesniemi, J., Niemel, M., Yl-Herttuala, S., Kovanen, P. T., and Frsen,

J. Smooth muscle cell foam cell formation, apolipoproteins, and abca1 in intracranial aneurysms: Implications for lipid accumulation as a promoter of aneurysm wall rupture. *Journal of Neuropathology and Experimental Neurology 75*, 7 (2016), 689–699.

[107] ORDEJÓ, P., DRABOLD, D. A., GRUMBACH, M. P., AND MARTIN, R. M. Unconstrained Minimization Approach for Electronic Computations That Scales Linearly with System Size. *Physical Review B 48* (1993), 14646.

[108] OTANI, T., NAKAMURA, M., FUJINAKA, T., HIRATA, M., KURODA, J., SHIBANO, K., AND WADA, S. Computational fluid dynamics of blood flow in coil-embolized aneurysms: effect of packing density on flow stagnation in an idealized geometry. *Medical & biological engineering & computing 51*, 8 (2013), 901–910.

[109] OUBEL, E., CRAENE, M. D., PUTMAN, C. M., CEBRAL, J. R., AND FRANGI, A. F. Analysis of intracranial aneurysm wall motion and its effects on hemodynamic patterns. In *Medical Imaging 2007: Physiology, Function, and Structure from Medical Images* (2007), vol. 6511, International Society for Optics and Photonics, p. 65112A.

[110] PAPAIOANNOU, T. G., AND STEFANADIS, C. Vascular wall shear stress: basic principles and methods. *Hellenic J Cardiol 46*, 1 (2005), 9–15.

[111] Piccinelli, M., Steinman, D. A., Hoi, Y., Tong, F., Veneziani, A., and Antiga, L. Automatic neck plane detection and 3d geometric characterization of aneurysmal sacs. *Annals of BIomedical Engineering 40*, 10 (2012), 2188–2211.

[112] Plimpton, S. J. Fast Parallel Algorithms for Short-Range Molecular Dynamics. *Journal of Computational Physics 117* (1995), 1.

[113] Potters, W. V., Marquering, H. A., VanBavel, E., and Nederveen, A. J. Measuring wall shear stress using velocity-encoded mri. *Current Cardiovascular Imaging Reports 7*, 4 (2014), 9257.

[114] Qiu, J., Zheng, Y., Hu, J., Liao, D., Gregersen, H., Deng, X., Fan, Y., and Wang, G. Biomechanical regulation of vascular smooth muscle cell functions: from in vitro to in vivo understanding. *Journal of The Royal Society Interface 11*, 90 (2014), 20130852.

[115] R Development Core Team. *R: A Language and Environment for Statistical Computing.* R Foundation for Statistical Computing, Vienna, Austria, 2011.

[116] Rinne, J., Hernesniemi, J., Puranen, M., and Saari, T. Multiple intracranial aneurysms in a defined population: prospective angiographic and clinical study. *Neurosurgery 35*, 5 (1994), 803–808.

[117] ROCHA, A. R. *Theoretical and Computational Aspects of Electronic Transport at the Nanoscale*. PhD thesis, University of Dublin, Trinity College, 2007.

[118] RUNGGER, I., AND SANVITO, S. Algorithm for the Construction of Self-Energies for Electronic Transport Calculations Based on Singularity Elimination and Singular Value Decomposition. *Physical Review B 78* (2008), 035407.

[119] SAWYER, D. M., PACE, L. A., PASCALE, C. L., KUTCHIN, A. C., ONEILL, B. E., STARKE, R. M., AND DUMONT, A. S. Lymphocytes influence intracranial aneurysm formation and rupture: role of extracellular matrix remodeling and phenotypic modulation of vascular smooth muscle cells. *Journal of neuroinflammation 13*, 1 (2016), 185.

[120] SCHAFHITZEL, T., VOLLRATH, J. E., GOIS, J. P., WEISKOPF, D., CASTELO, A., AND ERTL, T. Topology-preserving $\lambda2$-based vortex core line detection for flow visualization. In *Computer Graphics Forum* (2008), vol. 27, Wiley Online Library, pp. 1023–1030.

[121] SCHAFTENAAR, G., AND NOORDIK, J. H. *Journal of Computer-Aided Molecular Design 14* (2000), 123.

[122] SFORZA, D. M., PUTMAN, C. M., AND CEBRAL, J. R. Hemodynamics of cerebral aneurysms. *Annual review of fluid mechanics 41* (2009), 91–107.

[123] SHANNON, C. E. A mathematical theory of communication. *ACM SIGMOBILE Mobile Computing and Communications Review 5*, 1 (2001), 3–55.

[124] Soler, J. M., Artacho, E., Gale, J. D., García, A., Junquera, J., Ordejón, P., and Sánchez-Portal, D. The SIESTA Method for Ab Initio Order-N Materials Simulation. *Journal of Physics: Condensed Matter 14* (2002), 2745.

[125] Sujudi, D., and Haimes, R. Identification of swirling flow in 3-d vector fields. In *12th Computational Fluid Dynamics Conference* (1995), p. 1715.

[126] Sunderland, K., Haferman, C., Chintalapani, G., and Jiang, J. Vortex analysis of intra-aneurismal flow in cerebral aneurysms. *Computational and Mathematical Methods in Medicine 2016* (2016).

[127] Tibshirani, R. Regression shrinkage and selection via the lasso. *Journal of the Royal Statistical Society. Series B (Methodological)* (1996), 267–288.

[128] Tibshirani, R., Hastie, T., Narasimhan, B., and Chu, G. Diagnosis of multiple cancer types by shrunken centroids of gene expression. *Proceedings of the National Academy of Sciences 99*, 10 (2002), 6567–6572.

[129] Turjma, A. S., Turjman, F., and Edelman, E. R. Role of fluid dynamics and inflammation in intracranial aneurysm formation. *Circulation 129*, 3 (2014), 373–382.

[130] Tzima, E., Irani-Tehrani, M., Kiosses, W. B., Dejana, E., Schultz, D. A., Engelhardt, B., Cao, G., DeLisser, H., and Schwartz, M. A.

A mechanosensory complex that mediates the endothelial cell response to fluid shear stress. *Nature 437*, 7057 (2005), 426.

[131] UHANA FRÖSEN, TULAMO, R., PAETAU, A., LAAKSAMO, E., KORJA, M., LAAKSO, A., MIKANIEMELÄ, AND HERNESNIEMI, J. Saccular intracranial aneurysm: pathology and mechanisms. *Acta Neuropathologica 123*, 6 (Jun 2012), 773–786.

[132] UZARSKI, J. S., SCOTT, E. W., AND MCFETRIDGE, P. S. Adaptation of endothelial cells to physiologically-modeled, variable shear stress. *PloS one 8*, 2 (2013), e57004.

[133] VALEN-SENDSTAD, K., AND STEINMAN, D. Mind the gap: impact of computational fluid dynamics solution strategy on prediction of intracranial aneurysm hemodynamics and rupture status indicators. *American Journal of Neuroradiology* (2013).

[134] VARBLE, N., TUTINO, V., YU, J., SONIG, A., SIDDIQUI, A., DAVIES, J., AND MENG, H. Shared and distinct rupture disciminants of small and large intracranial. *Stroke 49* (2018), 856–864.

[135] VLAK, M. H., ALGRA, A., BRANDENBURG, R., AND RINKEL, G. J. Prevalence of unruptured intracranial aneurysms, with emphasis on sex, age, comorbidity, country, and time period: a systematic review and meta-analysis. *The Lancet Neurology 10*, 7 (2011), 626–636.

[136] WATTON, P., SELIMOVIC, A., RABERGER, N. B., HUANG, P., HOLZAPFEL, G., AND VENTIKOS, Y. Modelling evolution and the evolving mechanical environment of saccular cerebral aneurysms. *Biomechanics and modeling in mechanobiology 10*, 1 (2011), 109–132.

[137] WEN, J., DING, G., JIANG, W., WANG, Q., AND ZHENG, T. Numerical simulation of compliant artery bypass grafts using fluid–structure interaction framework. *Asaio Journal 60*, 5 (2014), 533–540.

[138] WILLIAMS, L. N., AND BROWN, R. D. Management of unruptured intracranial aneurysms. *Neurology: Clinical Practice 3*, 2 (2013), 99–108.

[139] WOLF, F., VOGT, F., SCHMITZ-RODE, T., JOCKENHOEVEL, S., AND MELA, P. Bioengineered vascular constructs as living models for in vitro cardiovascular research. *Drug discovery today 21*, 9 (2016), 1446–1455.

[140] XIANG, J., NATARAJAN, S. K., TREMMEL, M., MA, D., MOCCO, J., HOPKINS, L. N., SIDDIQUI, A. H., LEVY, E. I., AND MENG, H. Hemodynamic–morphologic discriminants for intracranial aneurysm rupture. *Stroke 42*, 1 (2011), 144–152.

[141] XIANG, J., SIDDIQUI, A., AND MENG, H. The effect of inlet waveforms on computational hemodynamics of patient-specific intracranial aneurysms. *Journal of biomechanics 47*, 16 (2014), 3882–3890.

[142] XIONG, G., FIGUEROA, C. A., XIAO, N., AND TAYLOR, C. A. Simulation of blood flow in deformable vessels using subject-specific geometry and spatially varying wall properties. *International journal for numerical methods in biomedical engineering 27*, 7 (2011), 1000–1016.

[143] XU, L., GU, L., AND LIU, H. Exploring potential association between flow instability and rupture in patients with matched-pairs of ruptured–unruptured intracranial aneurysms. *Biomedical engineering online 15*, 2 (2016), 166.

[144] XU, L., LEE, T.-Y., AND SHEN, H.-W. An information-theoretic framework for flow visualization. *IEEE Transactions on Visualization and Computer Graphics 16*, 6 (2010), 1216–1224.

[145] YASUDA, R., STROTHER, C. M., TAKI, W., SHINKI, K., ROYALTY, K., PULFER, K., AND KARMONIK, C. Aneurysm volume-to-ostium area ratio: a parameter useful for discriminating the rupture status of intracranial aneurysms. *Neurosurgery 68*, 2 (2011), 310–318.

[146] ZHOU, G., ZHU, Y., YIN, Y., SU, M., AND LI, M. Association of wall shear stress with intracranial aneurysm rupture: systematic review and meta-analysis. *Scientific reports 7*, 1 (2017), 5331.

[147] ZOU, H., AND HASTIE, T. Regularization and variable selection via the elastic net. *J.R. Statist. Soc. B* (2005), 301–320.

Appendix A

Statistics

In this type of predictive modeling, there exists an input-output dataset (X,Y) $\in XxY$ w with an unknown probability distribution P. The goal of predictive modeling is to find a function $f_n : X \to Y$, that is determined using a training set (X$_1$, Y$_1$,...,(X$_n$, Y$_n$) of n random pairs distributed as (X,Y). A desirable solution of f_n is one that, given a new data-point $x \in X$, the resultant f_n(x) is an accurate prediction of the true output $y \in Y$. This desired outcomes not only relies on the chosen function's predictive accuracy, but also of the selecting of relevant variables that are capable of achieving desired predictions. For desired models, it is often preferred to find the prediction function that achieves the desired accuracy while using the minimal amount of variables required: i.e a *parsimonious* model. Brute-force methods of testing all variable combinations becomes increasingly unviable, especially when the

number of variables in a dataset is larger than the number of n data points (cases) available for analysis: often refereed to the "large p, small n paradigm". One type of methodology to determine a desired model is through the use of sparsity-based regularization methods [71, 127, 128, 147]

Section 1

Multiple logistic regression (MLR) analysis looks both to estimate the odds of a dichotomous outcome occurring, and to determine the impact of an individual variable (covariate) in relation to the other covariates in a model. The probability of an outcome occurring in MLR can be calculated as such:

$$\hat{p} = \frac{exp(b_0 + b_1X_1 + b_2X_2 + ... + b_pX_p)}{1 + exp(b_0 + b_1X_1 + b_2X_2 + ... + b_pX_p)} \tag{A.1}$$

$\hat{p}$ being the probability of the desired outcome, X_1 through X_p as the individual dependent variables applied to the model, and b_1 to b_p being each variable's (respective) regression coefficients. To determine the expected log odds ratios of the model's variables, the *logit* function of the above equation can be calculated:

$$logit[\hat{p}] = ln[\frac{\hat{p}}{1-\hat{p}}]$$

$$= ln\left[\frac{\frac{exp(b_0+b_1X_1+b_2X_2+...+b_pX_p)}{1+exp(b_0+b_1X_1+b_2X_2+...+b_pX_p)}}{1-\frac{exp(b_0+b_1X_1+b_2X_2+...+b_pX_p)}{1+exp(b_0+b_1X_1+b_2X_2+...+b_pX_p)}}\right]$$

$$= ln\left[\frac{\frac{exp(b_0+b_1X_1+b_2X_2+...+b_pX_p}{1+exp(b_0+b_1X_1+b_2X_2+...+b_pX_p}}{\frac{1}{1+exp(b_0+b_1X_1+b_2X_2+...+b_pX_p)}}\right] \tag{A.2}$$

$$= ln[exp(b_0 + b_1X_1 + b_2X_2 + ... + b_pX_p]$$

$$= b_0 + b_1X_1 + b_2X_2 + ... + b_pX_p$$

Taking the *logit* of the desired outcome's probability, transforms the occurrence of the event given Xs into a simplified linear function.

For each variable added to a regression model, the resultant R^2 (coefficient of multiple determination) may increase, indicating an improved fit of the data. However applying a large number of variables to a predictive model may result in over-fitting without a significantly large dataset: large p, small n paradigm. In such an event, the R^2 values, regression coefficients, and any statistical significance (p-values) determined may be misleading. To reduce the initial choices of variables in assessed predictive models, the correlation between variables were determined. The correlation of data can be determine by:

$$r_{jk} = \frac{s_{jk}}{s_j s_k} = \frac{\sum_{i=1}^{n}(x_{ij} - \overline{x}_j)(x_{ik} - \overline{x}_k)}{\sqrt{\sum_{i=1}^{n}(x_{ij} - \overline{x}_j)^2}\sqrt{\sum_{i=1}^{n}(x_{ik} - \overline{x}_k)^2}} \tag{A.3}$$

with r as the Pearson correlation coefficient between variables x_j and x_k, n as the sample size, and $\overline{x}$ is a variable sample mean. Correlations between the variables are often displayed via a correlation table:

$$R = \begin{bmatrix} 1 & r_{12} & r_{13} & \dots & r_{1p} \\ r_{21} & 1 & r_{23} & \dots & r_{2p} \\ r_31 & r_{32} & 1 & \dots & r_{3p} \\ \vdots & \vdots & \vdots & \ddots & \dots \\ r_{p1} & r_{p2} & r_{p3} & \dots & 1 \end{bmatrix}$$

Initial correlation analysis of all available geometric and hemodynamic variables was performed to eliminate highly correlated variables from analysis: i.e aneurysm volume and surface area are highly correlated so surface area was removed from analysis.

From the remaining variables, stepwise MLR was implemented to determine the parsimonious model. In stepwise regression, a linear regression is first performed for each variable X one at a time, and the variable with the highest R^2 is kept for the model. Next, a multiple regression step is performed with the kept variable and each remaining variable. The variable with the largest increase in R_2, if the p value of the R^2 is below a desired cuttoff (<0.05), is added to the model. The calculation of the p value of an increase in R^2 resulting from the increasing of X variable(s) from a to

b is as follows:

$$p_{ab} = \frac{(R_b^2 - R_a^2)/(b - a)}{(1 - R_b^2)/(n - b - 1)} \tag{A.4}$$

with the total sample size n.

Each time a new variable is added to the model, the impact of removing any of the other variables (already added to the model) on outcomes is tested. The chosen (removed) variable is excluded from the model if it does not make R^2 significantly worse. This process is continued till adding any new variables does not increase R^2 and removing any X variables does not significantly decrease R^2

In the event that all of the independent variables in the model are completely uncorrelated with each other, the interpretation of coefficients are as such:

$$OR = exp(b_1)^z \tag{A.5}$$

Where z is the number of unit changes for a variable X, and OR is the odds ratio resultant from said change. When the variables are not uncorrelated, the $OR = exp^z b_1$ is expressed as the change of unit z for a variable *adjusted in relation to the impacts of the other variables in the model.* This stresses the need to assess collinearity between variables prior to model assessment.

in Section **??**.

Section 2

Limitations may arise in applying multiple logistic regression analysis to data sets with a large number of variables (inputs) in relation to the number of samples

According to Tibshirani et.al. [128] the NSC method shrinks each class' centroid toward the overall centroids after standardization using the within -class standard deviation for each variable. Standardizing the resultant centroid gives higher impact to variables whose expression is more stable withing samples of the same class.

For the NSC method: x_{ij} is the measured value for each input $i = 1, 2, ...p$ for each sample $j=1, 2, ...n$, with classes (in this case, rupture status) 1, 2, ...K and C_k as the indices of the n_k samples in class k. For each class k, its ith component of the centroid is $\overline{x}_{ik} = \sum_{j \in C_k} x_{jk}/n_k$, calculating the mean expression value in k for variable i. The ith component of the overall centroid is $\overline{x}_i = \sum_{j=1}^{n} x_{ij}/n$.

Taking into account the standardization of centroid, the standardization factor is calculated as:

$$d_{ik} = \frac{\overline{x}_{ik} - \overline{x}_i}{m_k \cdot (s_i + s_0)} \tag{A.6}$$

where s_i is the within-class standard deviation (for the variable i):

$$s_i^2 = \frac{1}{n-K} \sum_k \sum_{j \in C_k} (x_{ij} - \overline{x}_{ik})^2 m_k = \sqrt{\frac{1}{n_k} + \frac{1}{n}} \qquad (A.7)$$

The value of $m_k \cdot s_i$ equal to the estimated standard error of the numerator of d_{ik}. The value of s_0 is kept as a positive constant to protect against the occurrence of a large d_{ik} from variables with low levels of expression. The median value of s_i over the variables is used to set the value of s_0.

The calculation of $d$ik acts as a t statistics for the variables, comparing each class k to the overall centroid. This leads to a re-write of A.6 as:

$$\overline{x}_{ik} = \overline{x}_i + m_k(s_i + s_0)d_{ik} \qquad (A.8)$$

The value of d_{ik} is shrunk toward zero where:

$$\overline{x}'_{ik} = \overline{x}_i + m_k(s_i + s_0)d'_{ik} \qquad (A.9)$$

The level of shrinkage (thresholding) for d_{ik} is determined by a value Δ and is set to zero if the value is negative. The thresholding is calculated as:

$$d'_{ik} = sign(d_{ik})(|d_{ik}| - \Delta)_+ \tag{A.10}$$

with + identifying the positive aspect of the threshold.

The thresholding of d_{ik} results in the elimination of a number of variables from prediction model(s) as Δ increases. The remove a variable from a model was decided if, as (for a variable i), d_{ik} is shrunken to zero for all k which results in the centroid for variable $\bar{x}_i$ being the same for all k. This results that a variable does not contribute to the nearest-centroid calculation. The ideal value of Δ for a model is chosen by cross-validation.

Section 3

Elastic Net Regularization (ENR) overcomes some of the limitations of the LASSO selection method, primarily being able to accurately handle data sets with a high number of variables in relation to the sample size [42, 127]. Additionally, the ENR method is able to handle data sets with groups of highly correlated variables.

ENR solves two optimization problems:

$$\tilde{\beta} = \text{arg min}_{\beta} \sum_{i=1}^{N}(y_i - (X\beta)_i)^2$$

$$\text{subject to} \sum_{j=1}^{p}|\beta_j| \leq t_1 \text{ and } \sum_{j=1}^{p}\beta_j^2 \leq t_2 \tag{A.11}$$

were a penalty is places on the L_i norm($\sum_{j=1}^{p}|\beta_j|$) and the L_2 norm ($\sum_{j=1}^{p}\beta_j^2 \leq t_2$ of the regression coefficients. The purpose of these penalties are as follows: L_1 performs variable selection by setting some coefficients to 0, and L_2 works toward group selection by shrinking the coefficients of correlated variables toward each other. Re-writing equation A.11 in the Lagrangian form using two tuning parameters ($lambda_1$ and λ_2) is as follows:

$$\tilde{\beta} = \text{arg min}_{\beta} \left(\sum_{i=1}^{N}(y_i - (X\beta)_i)^2 + \lambda_1 \sum_{j=1}^{p}|\beta_j| + \lambda_2 \sum_{j=1}^{p}\beta_j^2 \right) \tag{A.12}$$

The choice of tuning parameter values is performed by analyzing an array of λ_2 values (0, 0.01, 0.1, 1, 10, and 100). For each value in the array, the LARS-EN algorithm calculates the resultant λ_1 value. The $lambda_1$ value that yields the smallest k-fold cross validation error, and its $lambda_2$ value used to generate it, are used as the tunning parameters for the ENR method.

Section 4

To assess the diagnostic ability of predictive model(s), a receiver operating characteristic curve (ROC) is often deployed (REFERENCES). The ROC curve assesses a model's predictive true positive rate (TPR) against its false positive rate (FPR) as a means to determine overall predictive strength (HANLEY). From a statistical perspective, ROC analysis can be considered as a plot of the power (probability of a test correctly rejecting the null hypothesis when an alternative hypothesis is true)

$$
\begin{aligned}
TPR &= \frac{\Sigma TruePositive}{\Sigma ConditionPositive} \\
FPR &= \frac{\Sigma FalsePpositive}{\Sigma ConditionNegative} \\
FNR &= \frac{\Sigma FalseNegative}{\Sigma ConditionPositive} \\
Specificity &= \frac{\Sigma TrueNegative}{\Sigma ConditionNegative}
\end{aligned}
\tag{A.13}
$$

When dealing with a binary classification, as per this study, the predictive test measure for each instance is denoted by a continuous random variable (x). Given a desired threshold (T), each instance is positive if x>T and negative if x<T. Setting the probability distribution functions of the positive and negative values of x to $f_p(x)$ and $f_n(x)$ respectively, the . Given this, TPR is calculated as:

$$TPR(T) = \int_{T}^{\infty} f_p(x)dx \tag{A.14}$$

and the FNR as:

$$FPR(T) = 1 - \int_{T}^{\infty} f_n(x)dx \tag{A.15}$$

The ROC curve is generated by plotting TPR(T) against FPR(T) parametrically, varying across T, or as a plot of:

$$ROC(T) = 1 - f_p(f_n^{-1}(1 - T)) \tag{A.16}$$

over T from [0,1] where $f_p^{-1}(1\text{-}T) = \inf$

Comparing the resultant ROC curves across multiple models provides the selection of the desired model based off of varying predictive accuracies. To quantify the predictive accuracy, the area under the curve (AUC) of the ROC curve is calculated, as it equals the probability of a classifier ranking a positive instance higher than a negative instance (both chosen at random).

$$A = \int_{\infty}^{-\infty} TPR(T)FPR'(T)dT$$

$$= \int_{-\infty}^{\infty} \int_{-\infty}^{\infty} I(T' > T)f_1(T')f_0(T)dT'dT = P(X_1 > X_0) \tag{A.17}$$

The initial integral has reversed boundaries due to larger T values having a lower value on the x-axis.

Section 5

Docendi eligendi sit et, pri ea dicam eligendi percipitur, has soleat dolores convenire te. Sed altera placerat an, id verterem abhorreant interesset mea. Eum at ceteros efficiantur. Eos id voluptaria efficiendi comprehensam.

In mel modo dicam vocibus, eruditi consectetuer vim no, cu quaestio instructior eum. Justo nostrud fuisset ea mea, eam an libris repudiandae vituperatoribus. Est choro corrumpit definitionem at. Vel sint adhuc vocibus ea, illud epicuri eos no. Sea simul officiis ea, et qui veri invidunt appellantur. Vix et eros ancillae pertinax.

Appendix B

Sample Code

The method for vortex identification for this study is a modification from previous work[126]. The calculation of vortex cores was based on in-house C++/Python codes derived from the open-source Vascular Modelling ToolKit (VMTK) [4]. Prior to any calculations, velocity data is first re-sampled onto a rectilinear grid whose voxel size is 0.2mm.

In the first step, the classic λ_2 method by Jeong and Hussain [72] was used to define the negative λ_2 region (*i.e* $\lambda_2 < 0$). Then, in the second step, vortex core lines were estimated by the method proposed by Sujudi and Haimes [125]. In essence, in the negative λ_2 region, a local velocity vector $\overline{v}$ lies along a vortex core line if the following two conditions hold: (1) the 3×3 spatial gradient matrix of $\overline{v}$ has two complex eigenvalues and one real eigenvalue and (2) the 3×3 spatial gradient matrix of $\overline{v}$ has
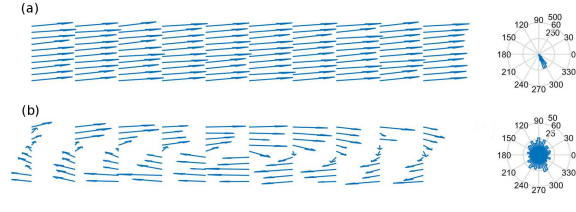
Figure B.1: Two examples illustrating the relationship between the angular histogram and NE: (a) a simple laminar flow case and (b) a rotational flow (eddy) case. In both cases, the right and left plots are the vector flow field and the histogram of angular vector direction, respectively. Vector fields were decimated by a factor of 3 for better visualization.

an eigenvector $\vec{\alpha}$ corresponding to the above-mentioned real eigenvalue. Now, if we define a new scalar value K as follows,

$$
K(x,y,z) = \begin{cases} |dot(\overline{v}, \vec{\alpha})|, & if\ \lambda_2 < 0 \\ \\ 0, & Otherwise \end{cases} \tag{B.1}
$$

where $|\cdot|$ is an absolute operator. Of note, in Eqn. 2, both the $\overline{v}$ and $\vec{\alpha}$ are normalized and therefore, the scalar field K defined above is bounded between 0 and 1. If the $K(x,y,z)$ is close to 1 then the location (x,y,z) is within the proximity of the vortex core line as suggested by Sujudi and Haimes [125].

In the third step, we calculated local normalized entropy (NE) of velocity directions [123] following work in the flow visualization literature (e.g. [97, 144]). The *NE* is close to 0 if the velocity direction closely concentrates one value out of N possible values (see Fig. B.1(a); NE=0.05). In contrast, the entropy measure *NE* becomes

66

0.95 if the probability of velocity directions is almost equally likely, as shown in Fig B.1(b). Given an arbitrary vexel located at *(x,y,z)* within the dome of an IA, we selected a fixed volume of interest (VOI; N_x x N_y x N_z; $N_x = N_y = N_z = 11$ in this study) centered at the voxel. One additional metric *H(x,y,z)* can be obtained by combining *K(x,y,z)* together with the *NE(x,y,z)* as follows,

$$H(x, y, z) = K(x, y, z) * NE(x, y, z) \tag{B.2}$$

H(x,y,z) is a scalar field representing the likelihood of residing within a vortex core region for a location (x,y,z). *H* also has a normalized range between 0 and 1. Thus, based on a fixed threshold, the vortex core region in this study can be obtained using the classic Marching-cube method [95]. in this study, 0.30 was used as the threshold for all data sets.

HelloWorld.c

```
// HelloWorld.c
// C program to display 'Hello, World!' in the terminal.
//
// Compilation:
// gcc -g -Wall HelloWorld.c -o HelloWorld.x
//
// Execution:
```

```c
// ./HelloWorld.x

// Standard headers
#include <stdio.h>

// main() begins
int main() {

  // Print the message
  printf("\n  Hello, World!\n\n");

  // Indicate the termination of main()
  return 0;
}
// main() ends
```

Appendix C

Letters of Permission

Include letters of permission from journal editors and/or other sources from which you may have used materials (images, information, etc.) in this this work.

These materials may also be submitted separately to the Graduate School as a single, well-organized PDF file.